TECHNICAL NOTE

D-794

TRANSONIC WIND-TUNNEL INVESTIGATION OF THE STATIC LONGITUDINAL AERODYNAMIC CHARACTERISTICS OF SEVERAL CONFIGURATIONS OF THE SCOUT VEHICLE AND OF A NUMBER OF RELATED MODELS

By Thomas C. Kelly

Langley Research Center
Langley Field, Va.

NATIONAL AERONAUTICS AND SPACE ADMINISTRATION
WASHINGTON
May 1961

NATIONAL AERONAUTICS AND SPACE ADMINISTRATION

TECHNICAL NOTE D-794

TRANSONIC WIND-TUNNEL INVESTIGATION OF THE STATIC LONGITUDINAL AERODYNAMIC CHARACTERISTICS OF SEVERAL CONFIGURATIONS OF THE SCOUT VEHICLE AND OF A NUMBER OF RELATED MODELS

By Thomas C. Kelly

SUMMARY

Results have been obtained in the Langley 8-foot transonic pressure tunnel at Mach numbers from 0.40 to 1.20 for several configurations of the Scout vehicle and for a number of related models. Tests extended over an angle-of-attack range from about -10° to 10° at a Reynolds number per foot of about 3.8×10^{6}.

Results indicated that for an early version of the Scout vehicle, a change in second-stage transition-flare half-angle from 5.2° to 8.2° had negligible effects on normal-force and pitch characteristics but caused a slight increase in the transonic drag rise.

Tests of various configurations of a 1/15-scale model of the four-stage Scout vehicle indicated that the addition of various protuberances increased the axial force noticeably and caused a slight forward movement in center-of-pressure location. The addition of low-aspect-ratio fins on the second-stage transition flare caused slight general increases in normal-force-curve slope, pitching-moment-curve slope, and axial force and moved the center of pressure forward by about 2 to 5 percent of the body length.

Results of tests of various configurations of a 1/10-scale model of a three-stage version of the Scout vehicle indicated that the addition of an afterbody flare to the fin-off configuration caused sizable increases in normal-force-curve slope and pitching-moment-curve slope, whereas addition of the same flare to the fin-on configuration had negligible effects.

INTRODUCTION

The Scout program of the National Aeronautics and Space Administration was established to provide a vehicle for space research that would be relatively low in cost, have a high degree of dependability, perform a variety of research missions, and that could be launched by using relatively simple ground handling equipment. The Scout vehicle which has been developed in this program is a four-stage solid-fuel rocket and is designed for orbital, vertical probe, and reentry missions.

As part of the vehicle development program, tests have been conducted in the Langley 8-foot transonic pressure tunnel to determine the static longitudinal aerodynamic characteristics for a number of Scout, and related, configurations. These tests were conducted through a Mach number range from 0.40 to 1.20 and an angle-of-attack range from about -10° to 10°. Reynolds numbers per foot for the tests were approximately 3.8×10^{6}.

Results for some similar models tested at supersonic speeds are available in references 1 to 3.

SYMBOLS

Aerodynamic force and moment data are referred to the body system of axes. Reference constants for the various configurations tested are presented in table I.

C_A axial-force coefficient, $\frac{\text{Axial force}}{qA}$

$C_{A,b}$ base axial-force coefficient, $\frac{\text{Base axial force}}{qA}$

C_m pitching-moment coefficient, $\frac{\text{Pitching moment}}{qAd}$

C_{m_α} pitching-moment-curve slope, $\frac{\partial C_m}{\partial \alpha}$, per deg (measured at $\alpha = 0^{\circ}$)

C_N normal-force coefficient, $\frac{\text{Normal force}}{qA}$

C_{N_α}	normal-force-curve slope, $\frac{\partial C_N}{\partial \alpha}$, per deg (measured at $\alpha = 0^\circ$)
d	body maximum cylindrical diameter, in
l	model overall length, measured from nose-cone apex to fin trailing edge, in.
M	Mach number
q	free-stream dynamic pressure, lb/sq ft
A	body maximum cross-sectional area, sq ft
x	distance, measured from nose-cone apex, in.
α	angle of attack of body center line, deg
R	Reynolds number per foot
r	radius of curvature, in.

Subscript:

cp	center of pressure

APPARATUS AND TESTS

Models

For purposes of clarity the various model configurations tested are separated into three general groups. Configuration numbers used herein were established prior to the tunnel tests and, because of additions and deletions during actual testing, may not follow an orderly arrangement.

1/15-scale four-stage research model configurations.- Drawings of two configurations of the 1/15-scale four-stage research model are presented in figure 1. The configurations, which represent early versions of proposed Scout vehicles, differ only in the second-stage flare angle and in overall length. These configurations are identical to the "small fin" configurations of reference 2.

1/15-scale four-stage Scout model configurations.- Drawings for one configuration of a 1/15-scale model of the four-stage Scout vehicle are presented in figure 2. Several configurations of this model were tested and are described as follows:

Configuration	Description
115	Body alone
215	Body plus first-stage delta fins
315	Body and delta fins plus antennas, wiring tunnels, and launch fittings (protuberances)
415	Body, delta fins, and protuberances plus second-stage stub fins rolled 45° with respect to delta fins
515	Body and delta fins plus second-stage stub fins rolled 45° with respect to delta fins
615	Body, delta fins, and protuberances plus second-stage stub fins in line with delta fins

1/10-scale three-stage Scout model configurations.- Drawings for the 1/10-scale three-stage Scout model and the various afterbody and fin configurations tested are presented in figure 3.

The several configurations tested are described as follows:

Configuration	Model description
110	Body alone
210	Body plus antennas and wiring tunnels
310	Body, antennas, and wiring tunnels plus delta fins
410	Body with 5° flared skirt plus antennas and wiring tunnels
510	Body with 5° flared skirt, antennas, and wiring tunnels plus delta fins
610	Body with 5° flared skirt
810	Body with 5° flared skirt, antennas, and wiring tunnels plus clipped delta fins
910	Body, antennas, and wiring tunnels plus clipped delta fins

With fins removed and flared skirt and protuberances on, configuration 410 represents the upper three stages of the Scout vehicle.

Photographs of various configurations from these three general groups are provided in figure 4.

Tests and Procedure

Tests were conducted in the Langley 8-foot transonic pressure tunnel over a Mach number range from 0.40 to about 1.20 and through an angle-of-attack range from 10° to -10° for the 1/15-scale models and from 6° to -6° for the 1/10-scale models. Test Reynolds numbers per foot varied from about 2.3×10^6 at a Mach number of 0.40 to 4.2×10^6 at a Mach number of 1.20.

No transition strips were used during tests of the 1/15-scale research models. However, for the 1/15-scale and 1/10-scale Scout models transition strips composed of No. 120 carborundum grains set in a plastic adhesive were employed at the forward antenna station for configurations having the antennas off. For configurations with antennas on, no transition strips were used.

Measurements

Normal force, axial force, and pitching moments were determined by means of an internal electrical strain-gage balance. Coefficients for the 1/15-scale models are based on a body maximum cross-sectional area of 0.0388 square foot and a reference length of 2.668 inches. Coefficients for the 1/10-scale models are based on a body cross-sectional area of 0.0524 square foot and a length of 3.10 inches. Moment-reference-center stations are provided in table I and are shown in figures 1 to 3.

Corrections

Effects of subsonic boundary interference in the slotted test section are considered negligible and no corrections for these effects have been applied. At supersonic speeds, the data are generally affected by boundary-reflected disturbances which occur at Mach numbers from slightly over 1.03 to those at which the disturbances are reflected downstream of the model base. For the present tests, the model lengths and tunnel power restrictions precluded the attainment of a Mach number at which the models would be reflection-free. Therefore, the results presented for the 1/15-scale models at a Mach number of 1.20 and for the 1/10-scale models at a Mach number of 1.11 may be subject to error resulting from shock reflection and are included primarily to allow comparison with results obtained at higher speeds.

Axial-force data presented herein have been adjusted to correspond to the condition of free-stream static pressure acting at the model base and in the balance chamber.

Accuracy

Based upon a consideration of factors affecting the accuracy of the results, measured coefficients are estimated to be accurate within the following limits:

M	Accuracy of 1/15-scale models for -		
	C_N	C_A	C_m
0.40 1.20	±0.18 ±.05	±0.03 ±.01	±0.16 ±.04

M	Accuracy of 1/10-scale models for -		
	C_N	C_A	C_m
0.40 1.11	±0.14 ±.04	±0.02 ±.006	±0.10 ±.03

Model angle of attack is estimated to be accurate within ±0.1°.

PRESENTATION OF RESULTS

A list of figures presenting results of this investigation is given below. In order to facilitate presentation of the data, staggered scales have been used in some of the figures and care should be taken in selecting the proper zero axis for each curve. With regard to the center-of-pressure location plotted against angle of attack in figures 6, 8, 9, and 12 to 14, it should be noted that the flagged test points were computed using C_{M_α} and C_{N_α} which were taken at an angle of attack of 0°.

DISCUSSION

1/15-Scale Four-Stage Research Model

Results for the 1/15-scale four-stage research model, presented in figure 6 and summarized in figure 7, show that a change in second-stage transition-flare angle had only slight effects on the normal-force, pitch, and center-of-pressure characteristics for both the fin-on and fin-off conditions (fig. 7(a)). As would be expected, addition of the fins causes sizable increases in the normal-force-curve slope and in the stability level, and thus causes a rearward shift in center-of-pressure location which amounts to about 40 percent of the body length.

Comparison of axial-force coefficients for the various configurations (fig. 7(b)) indicates that the change in transition-flare angle from 5.2° to 8.2° is accompanied by a slight increase in the transonic drag rise. A comparison of base axial-force coefficients for the various configurations shows that no effects on base axial force result from the change in transition-flare angle.

1/15-Scale Four-Stage Scout Model

The effects of adding fins and protuberances to a 1/15-scale model of the Scout vehicle are presented in figures 8 and 9 and are summarized in figures 10 and 11. Results given in figure 10(a) indicate that addition of the first-stage fins causes sizable increases in normal-force-curve slope and in the stability level, and therefore results in a considerable rearward shift in center-of-pressure location. The further addition of protuberances has only small effects which cause a slight forward shift in center-of-pressure location.

L
1
1
4
6

Axial-force results, presented in figure 10(b), show that addition of the first-stage fins increases the axial-force coefficient throughout the Mach number range by about 50 percent. Further addition of the protuberances causes an increase in axial-force coefficient of about 0.09 throughout the Mach number range. In the simulation of various protuberances for the model, cylindrical rods were used to represent telemeter antennas. (See fig. 4(e).) For the full-scale vehicle, the telemeter antennas are more streamlined in cross section; therefore, the incremental axial-force coefficients associated with addition of the protuberances are probably slightly higher for the model than would be expected on the full-scale vehicle because of the relatively high-drag cross-sectional shape of the simulated antennas.

The effects of adding stub fins to the second stage of the basic Scout model, either in line with the first-stage fins or rolled 45° with respect to the first-stage fins, are shown in figures 9 and 11. The results presented in figure 11(a) indicate that addition of the stub fins in either orientation causes a slight increase in C_{N_α}, and a more pronounced increase in C_{m_α}, and therefore results in a forward shift in center-of-pressure location that varies from about 2 percent of the body length at a Mach number of 0.40 to about 5 percent of the body length at a Mach number of 1.20.

Axial-force results, presented in figure 11(b), show that addition of the stub fins causes a slight general increase in axial-force coefficient throughout the Mach number range, as would be expected. Variations in base axial-force coefficients due to addition of the stub fins are seen to be generally negligible.

1/10-Scale Three-Stage Scout Model

The effects of fins, protuberances, and the flared afterbody on the aerodynamic characteristics of the 1/10-scale three-stage Scout model are presented in figures 12 to 14 and are summarized in figures 15 to 17.

Results are presented in figure 15(a) which show the effects of adding protuberances and either delta or clipped-delta fins to the model with a cylindrical afterbody. These results show that adding antennas and wiring tunnels to the three-stage body alone has no effect on C_{N_α}, but increases C_{m_α} slightly, and therefore results in a forward shift in center-of-pressure location which amounts to about 4 percent of the body length. Addition of fins results in sizable increases in C_{N_α} and in stability level, as would be expected, and shifts the center of pressure rearward by about 40 and 50 percent of the body length for the configurations with clipped-delta and delta fins, respectively.

Axial-force results, presented in figure 15(b), show effects due to addition of the fins and protuberances similar to those noted for the 1/15-scale models.

Results given in figure 16 show the effects of adding fins and protuberances to the configuration with the flared-skirt afterbody. These effects are, in general, qualitatively similar to those noted for the configuration with the cylindrical afterbody.

Figure 17 presents aerodynamic characteristics in pitch for several configurations. Comparisons of these results indicate the effects of adding an afterbody flare for the configurations with and without the delta fins. The most interesting effects to be noted from the comparisons are that although sizable variations are seen to result from adding a flared skirt to the fin-off configuration, negligible effects result from adding the flared skirt to the fin-on configuration. For example, adding the flared skirt to the fin-off configuration causes an increase in C_{N_α} that varies from 49 percent at a Mach number of 0.40 to 70 percent at a Mach number of 1.20. Since this increase in normal force is associated with the addition of a surface located at the base of the body, the stability level is increased, and the center of pressure moves rearward about 25 percent of the body length. Similar addition of the flared skirt to the fin-on configuration, however, causes only slight random effects to occur in the normal-force, pitch, and center-of-pressure characteristics (fig. 17(a)).

Although not presented as a separate comparison, addition of the flared skirt to the configuration with the clipped delta fins results in variations similar to those noted above. The effects may be seen by comparing results for configuration 910 (flare off) presented in figure 15 with those for configuration 810 (flare on) given in figure 16.

Examination of figure 3 indicates the probable reason for the difference in the effects caused by adding the flared skirt to the fin-on

configuration and to the fin-off configuration. It may be seen that in the process of adding the flared skirt to the configurations having fins, a portion of the fin (about 16 percent of the exposed area for the delta-fin configuration) is covered by the skirt. The loss in normal force associated with this fin coverage is apparently equal to the increase in normal force resulting from addition of the flared skirt; therefore, the overall effects of adding a flared skirt are negligible for this combination of fin and skirt.

Axial-force results (fig. 17(b)) indicate that addition of the flared skirt causes a slight increase in the transonic drag rise for both the fin-on and fin-off configurations. Base axial-force coefficients for the fin-on and fin-off configurations are increased considerably as a result of adding the flared skirt.

CONCLUDING REMARKS

Results of tests of a 1/15-scale model of the Scout vehicle and of several related models have indicated that a change in second-stage transition-flare half-angle from 5.2° to 8.2° had negligible effects on normal-force, center-of-pressure, and pitch characteristics and caused a slight increase in the transonic drag rise for configurations of a 1/15-scale model of an early version of the Scout vehicle.

Results from tests of a 1/15-scale model of the Scout vehicle have indicated that the addition of various protuberances increased the axial force noticeably and caused a slight forward movement in center-of-pressure location. The addition of low-aspect-ratio fins on the second-stage transition flare, either in line with the first-stage fins or rolled 45° with respect to the first-stage fins, caused slight general increases in normal-force-curve slope, pitching-moment-curve slope, and axial force, and moved the center of pressure forward by about 2 to 5 percent of the body length.

Results from tests of a 1/10-scale model of a three-stage version of the Scout vehicle have indicated that the addition of protuberances had effects similar to those noted for the four-stage Scout model. Addition of an afterbody flare to the fin-off configuration caused sizable increases in normal-force-curve slope and pitching-moment-curve slope, whereas addition of the same flare to the fin-on configuration had negligible effects.

Langley Research Center,
National Aeronautics and Space Administration,
Langley Field, Va., January 30, 1961.

REFERENCES

1. Keynton, Robert J., and Fichter, Ann B.: Investigation of the Aerodynamic Characteristics of Two Preliminary Designs of Scout Research Vehicle at Mach Numbers From 1.77 to 4.65. NASA TN D-821, 1961.

2. Jernell, Lloyd S., and Wong, Norman: Investigation of the Static Longitudinal Stability Characteristics of a 0.067-Scale Model of a Four-Stage Configuration of the Scout Research Vehicle at Mach Numbers of 2.29, 2.96, 3.96, and 4.65. NASA TN D-554, 1960.

3. Robinson, Ross B.: Aerodynamic Characteristics in Pitch and Sideslip of a 1/15-Scale Model of the Scout Vehicle at a Mach Number of 2.01. NASA TN D-793, 1961.

TABLE I.- MODEL REFERENCE CONSTANTS

Reference constants	1/15-scale four-stage research model		1/15-scale four-stage Scout model	1/10-scale three-stage Scout model
	5.2° flare half-angle	8.2° flare half-angle		
Reference area, A, sq ft	0.0388	0.0388	0.0388	0.0524
Reference length, d, in.	2.668	2.668	2.668	3.10
Model overall length (nose-cone apex to fin trailing edge), l, in.	57.125	55.795	57.214	48.582
Moment reference center, body station, in.	37.580	36.250	37.779	33.162
Moment reference center, x/l . . .	0.658	0.650	0.660	0.683

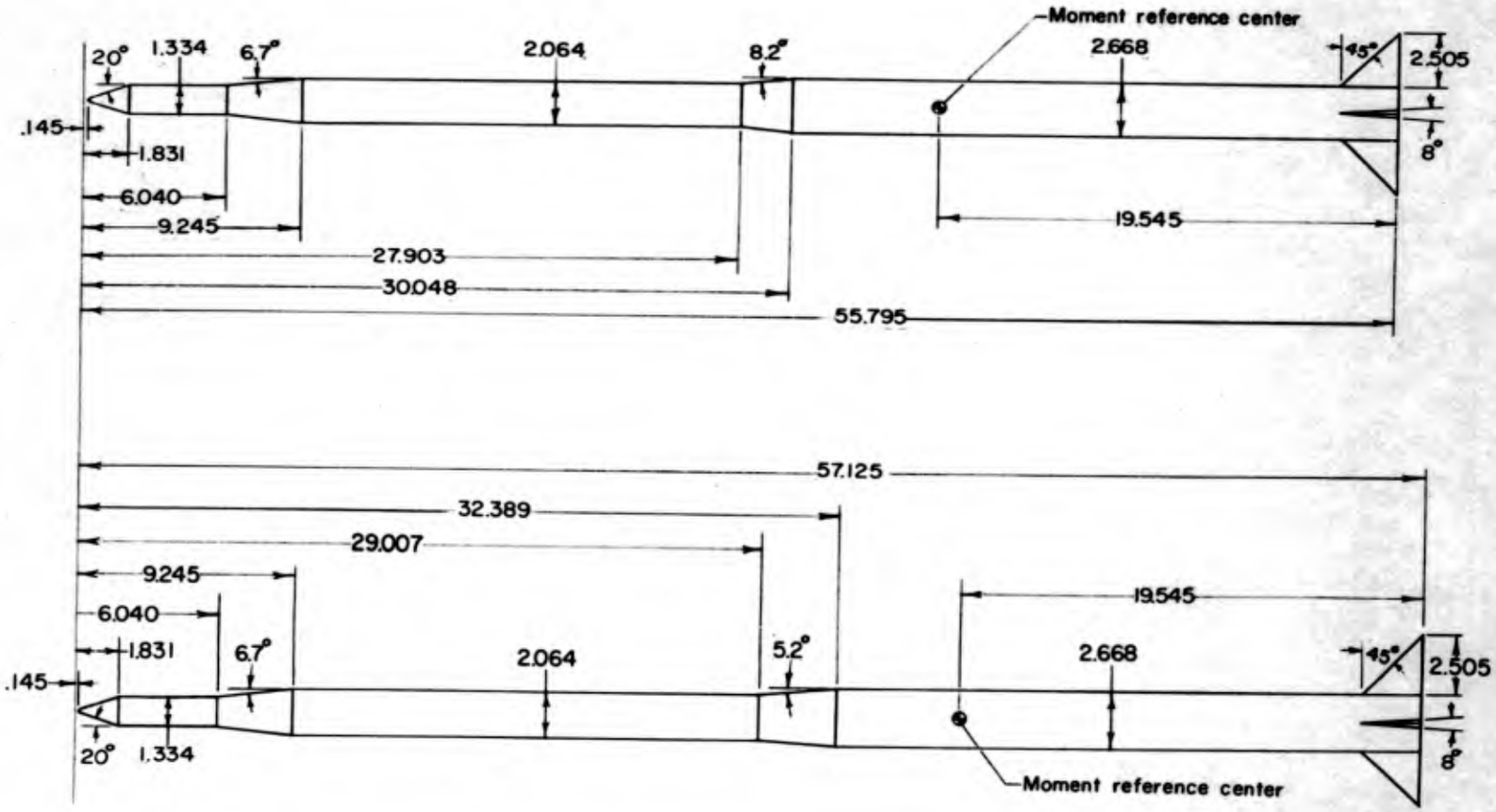

Figure 1.- Configurations of 1/15-scale four-stage research model. All dimensions are in inches unless otherwise noted.

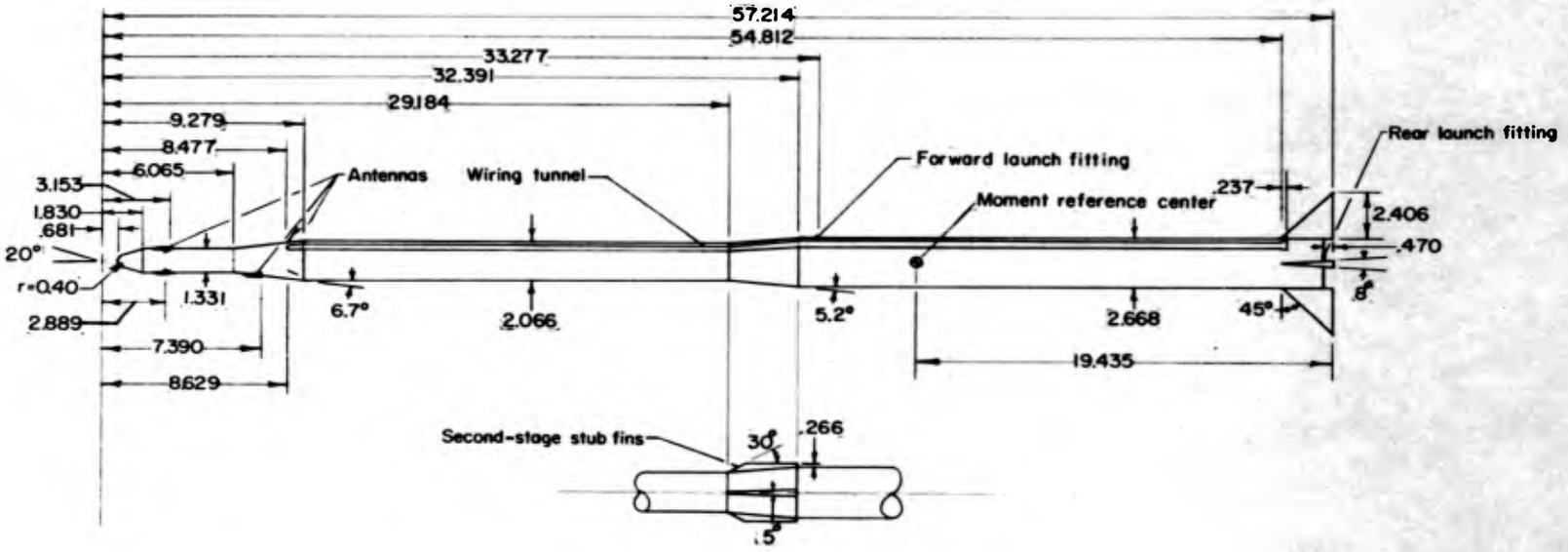

Figure 2.- Details of 1/15-scale four-stage Scout model. All dimensions are in inches unless otherwise noted.

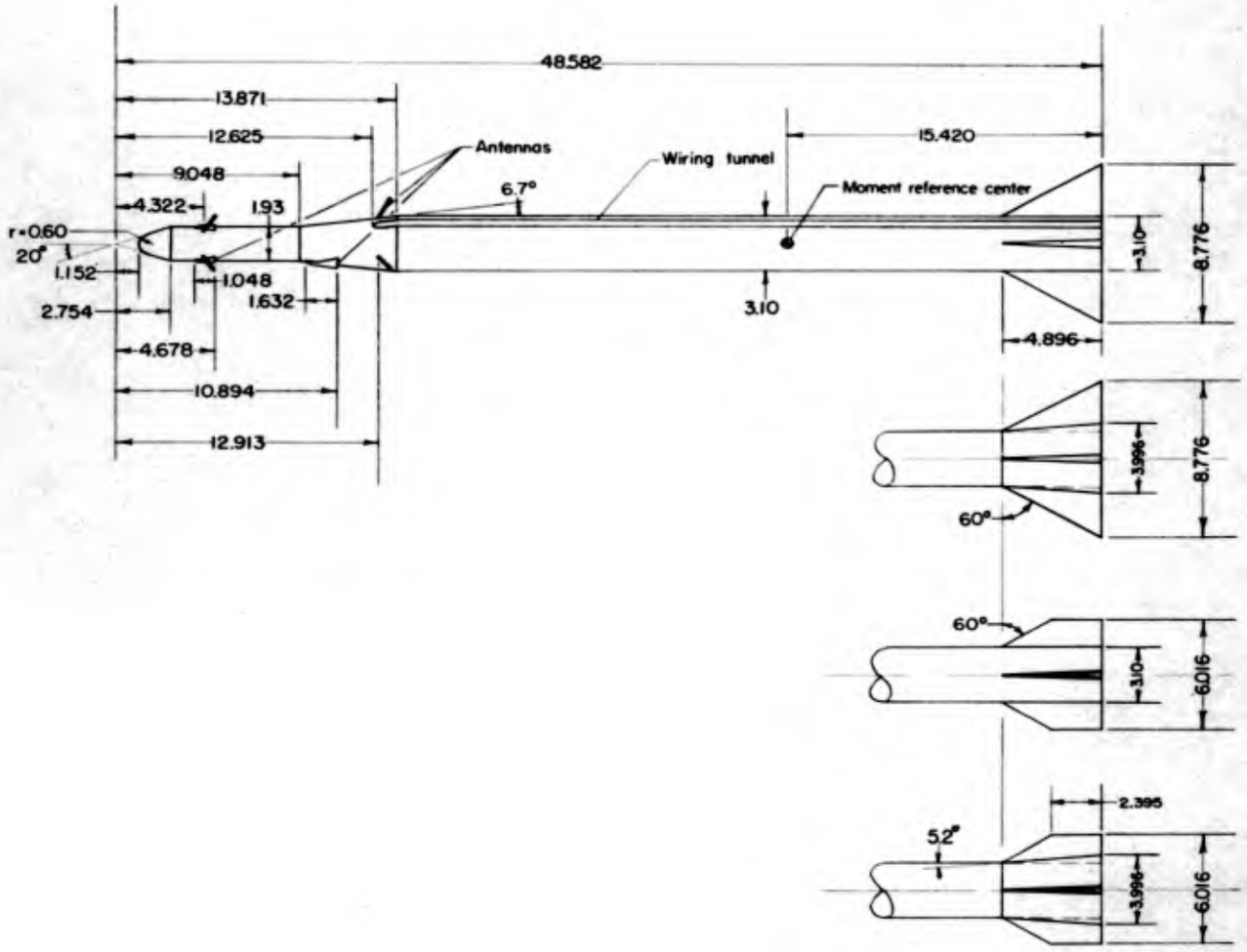

Figure 3.- Details of 1/10-scale three-stage Scout model and several afterbody configurations. All dimensions are in inches unless otherwise noted.

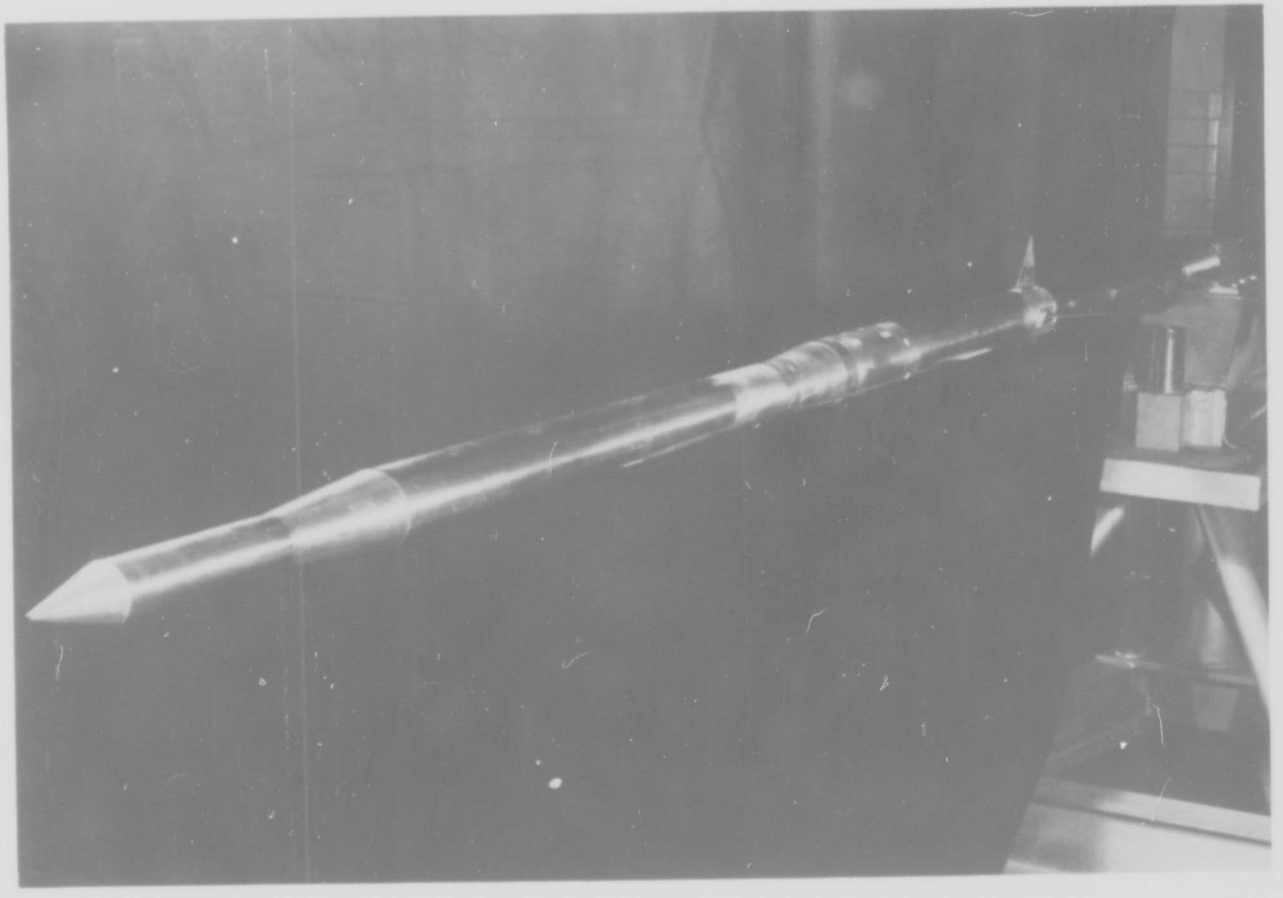

(a) 1/15-scale four-stage research model. L-59-3666

Figure 4.- Photographs of various configurations.

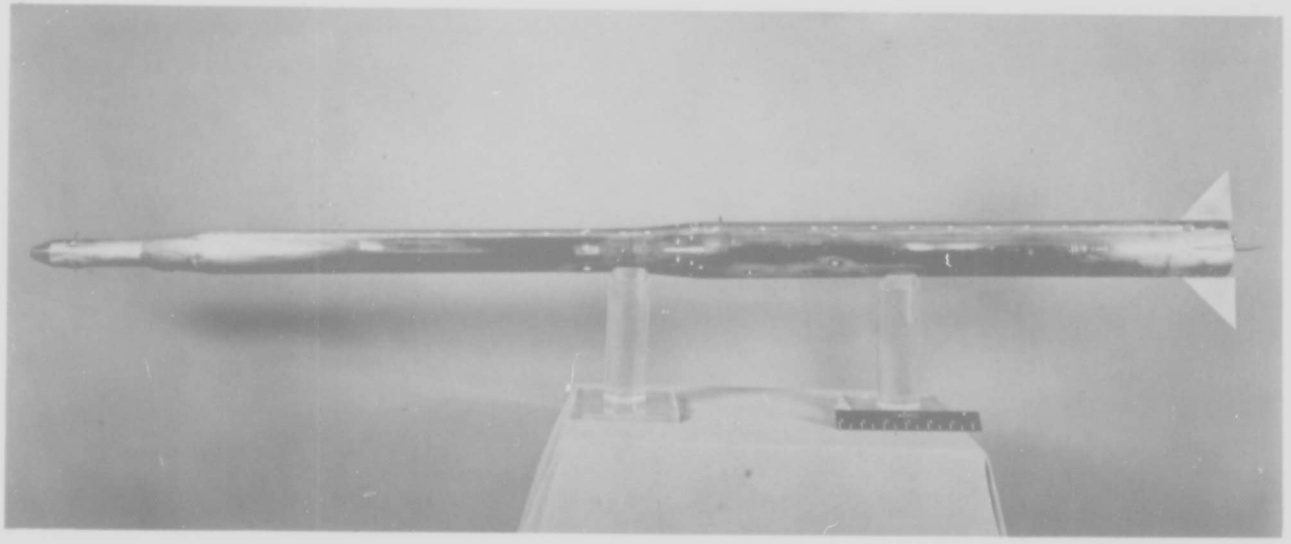

(b) 1/15-scale four-stage Scout model. Configuration 315. L-59-7668

Figure 4.- Continued.

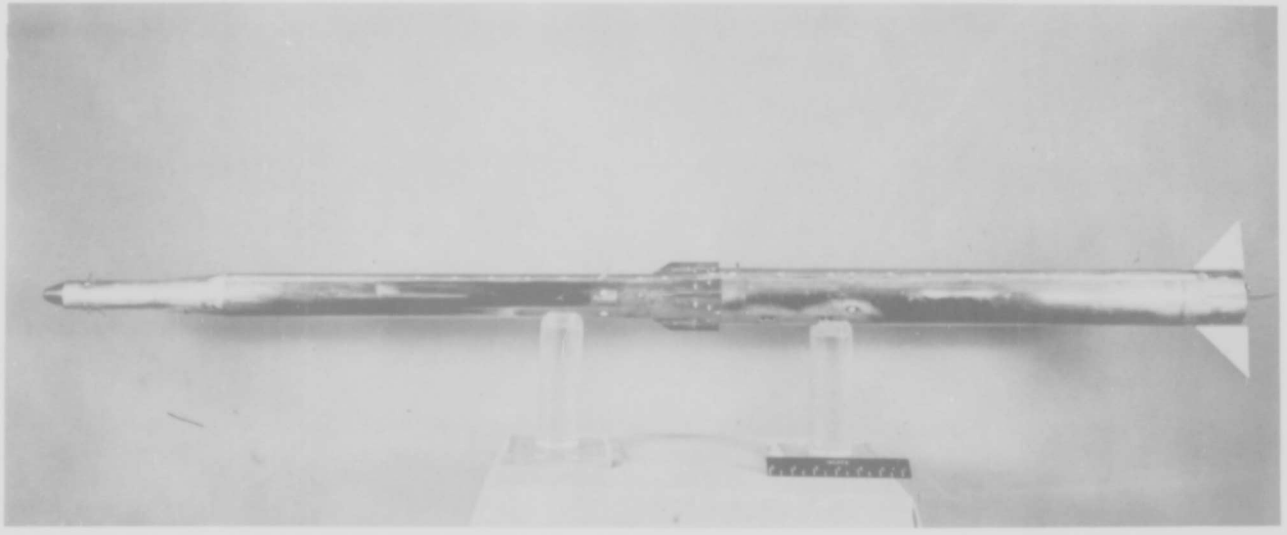

(c) 1/15-scale four-stage Scout model. Configuration 615. L-59-7669

Figure 4.- Continued.

(d) 1/10-scale three-stage Scout model. Configuration 510. L-59-6352

Figure 4.- Continued.

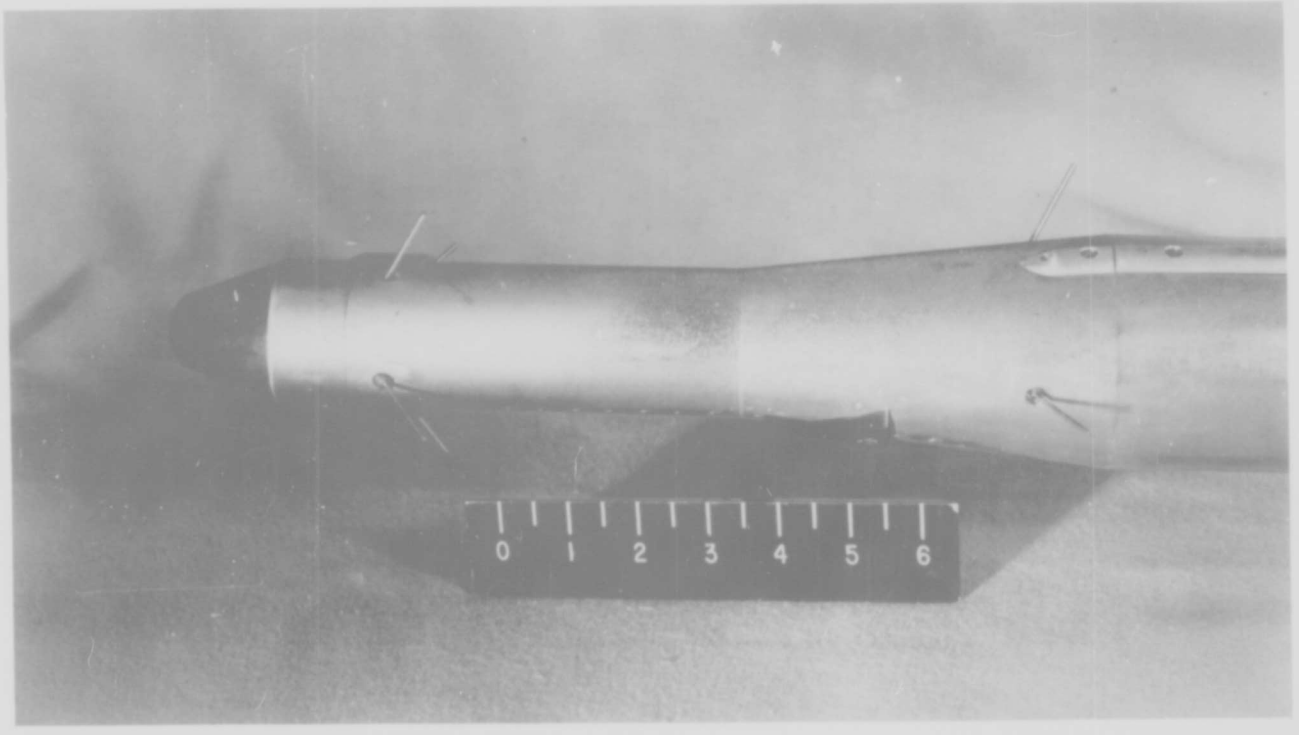

L-59-6354

(e) 1/10-scale three-stage Scout model. Forebody details, configurations having protuberances.

Figure 4.- Concluded.

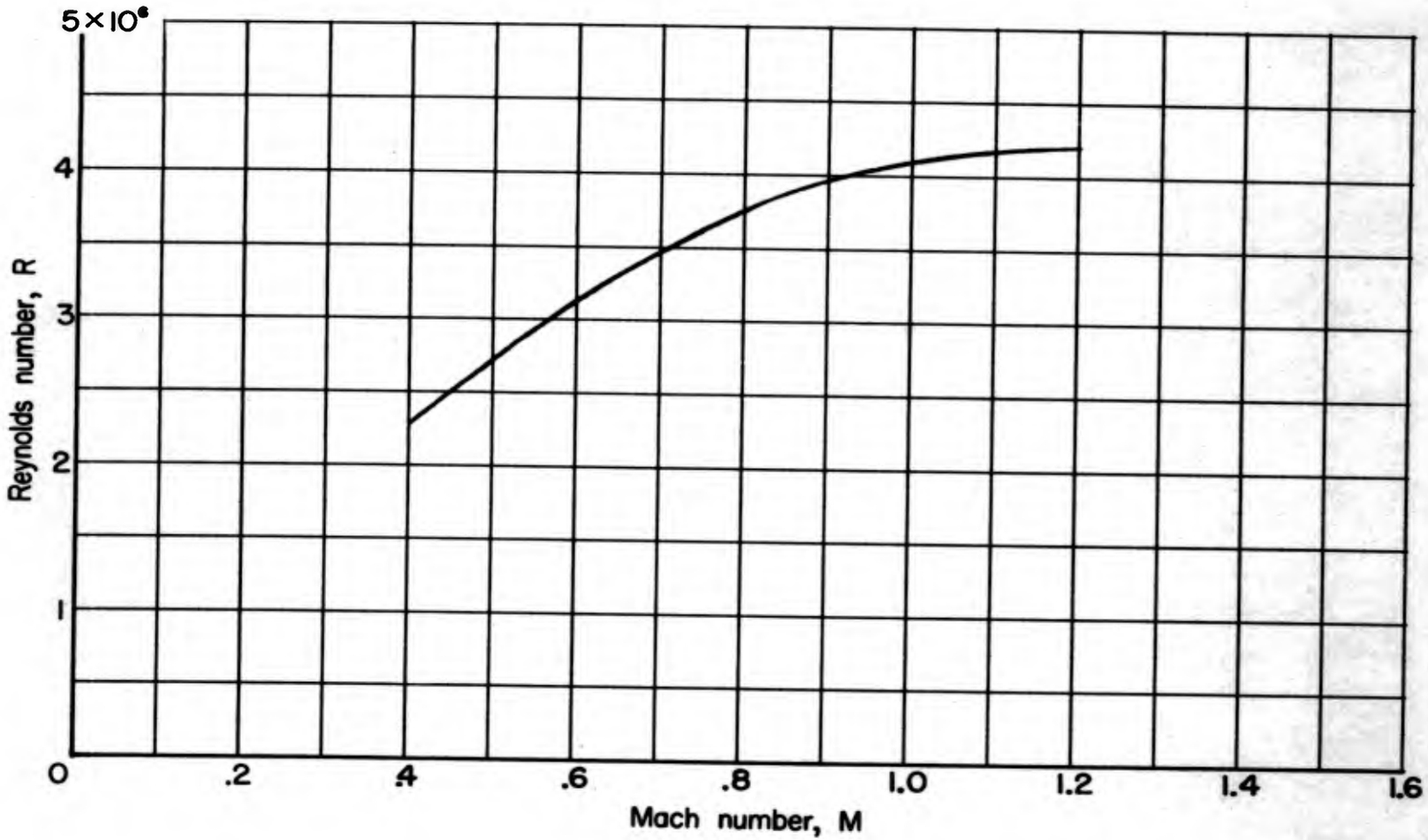

Figure 5.- Variation of test Reynolds number per foot with Mach number.

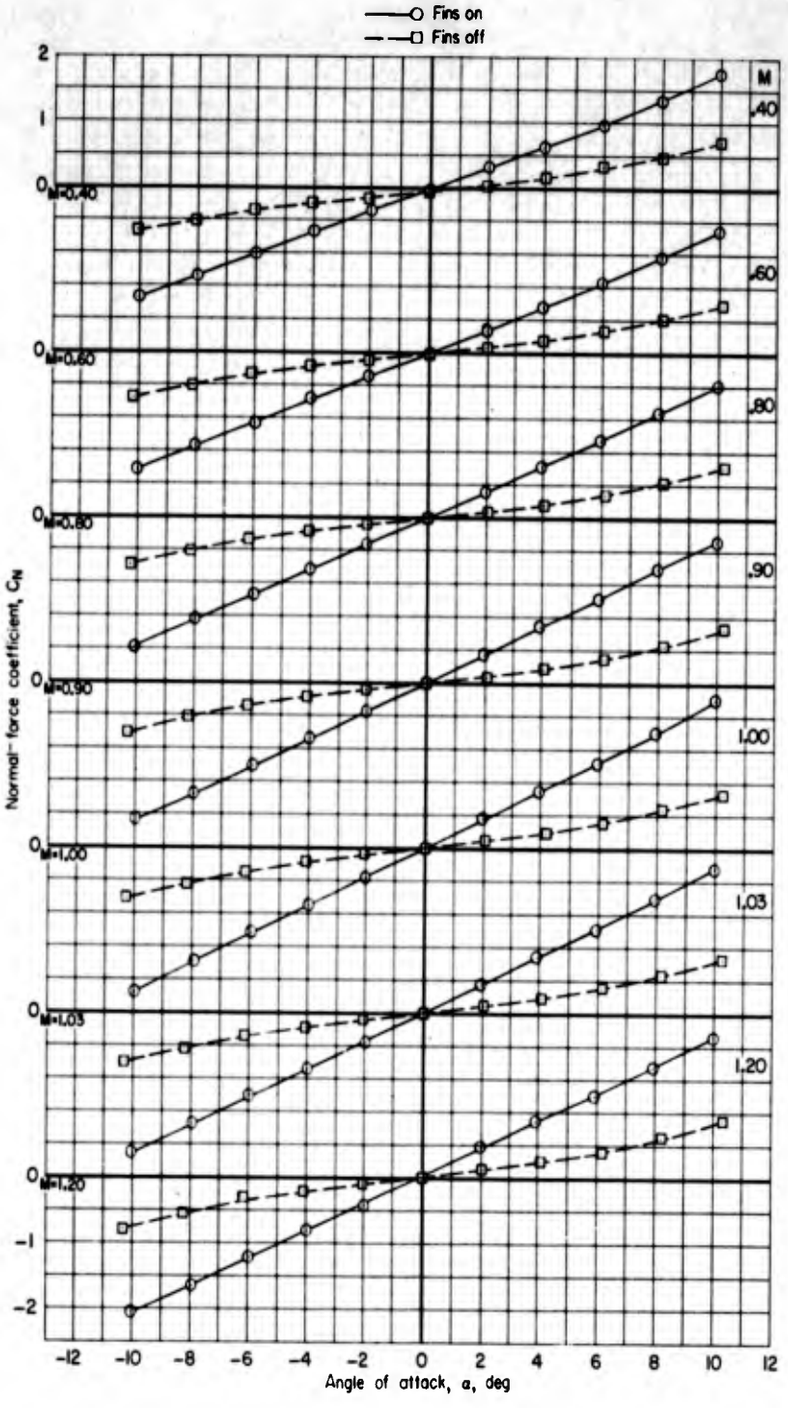

(a) C_N plotted against α; 5.2° flare half-angle.

Figure 6.- Effect of delta fins on aerodynamic characteristics in pitch for two transition flare angles. 1/15-scale four-stage research model.

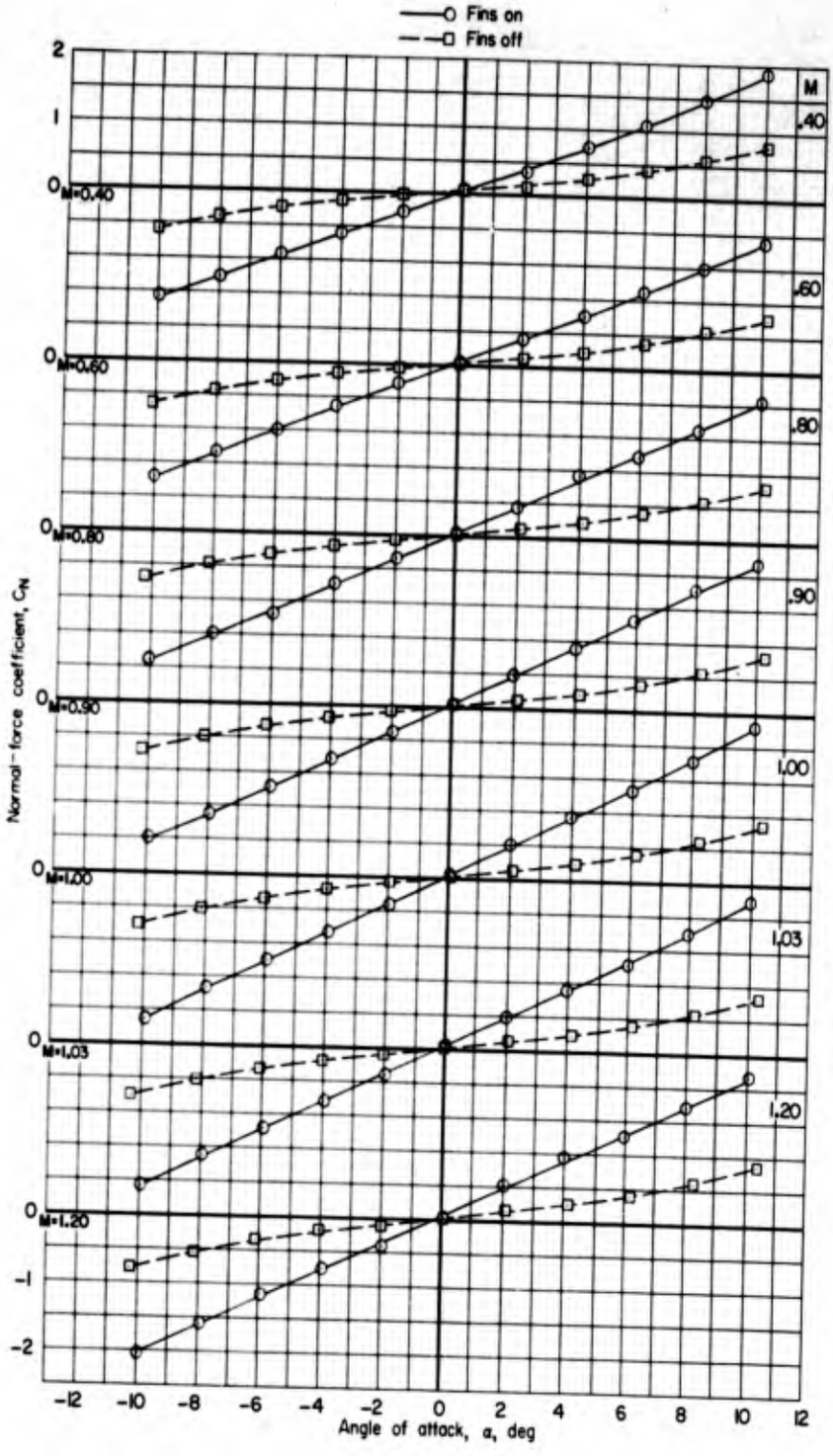

(b) C_N plotted against α; 8.2° flare half-angle.

Figure 6.- Continued.

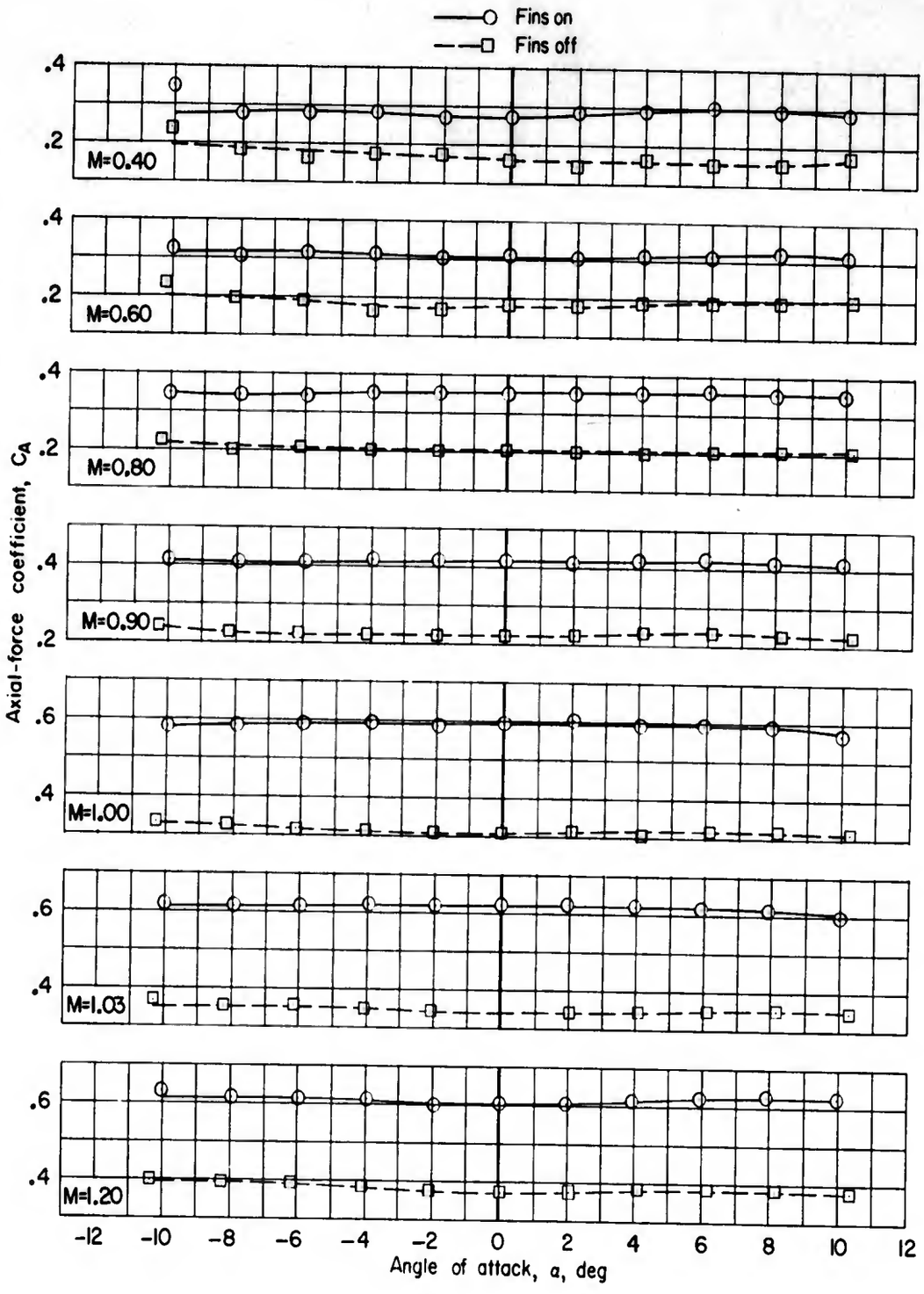

(c) C_A plotted against α; 5.2° flare half-angle.

Figure 6.- Continued.

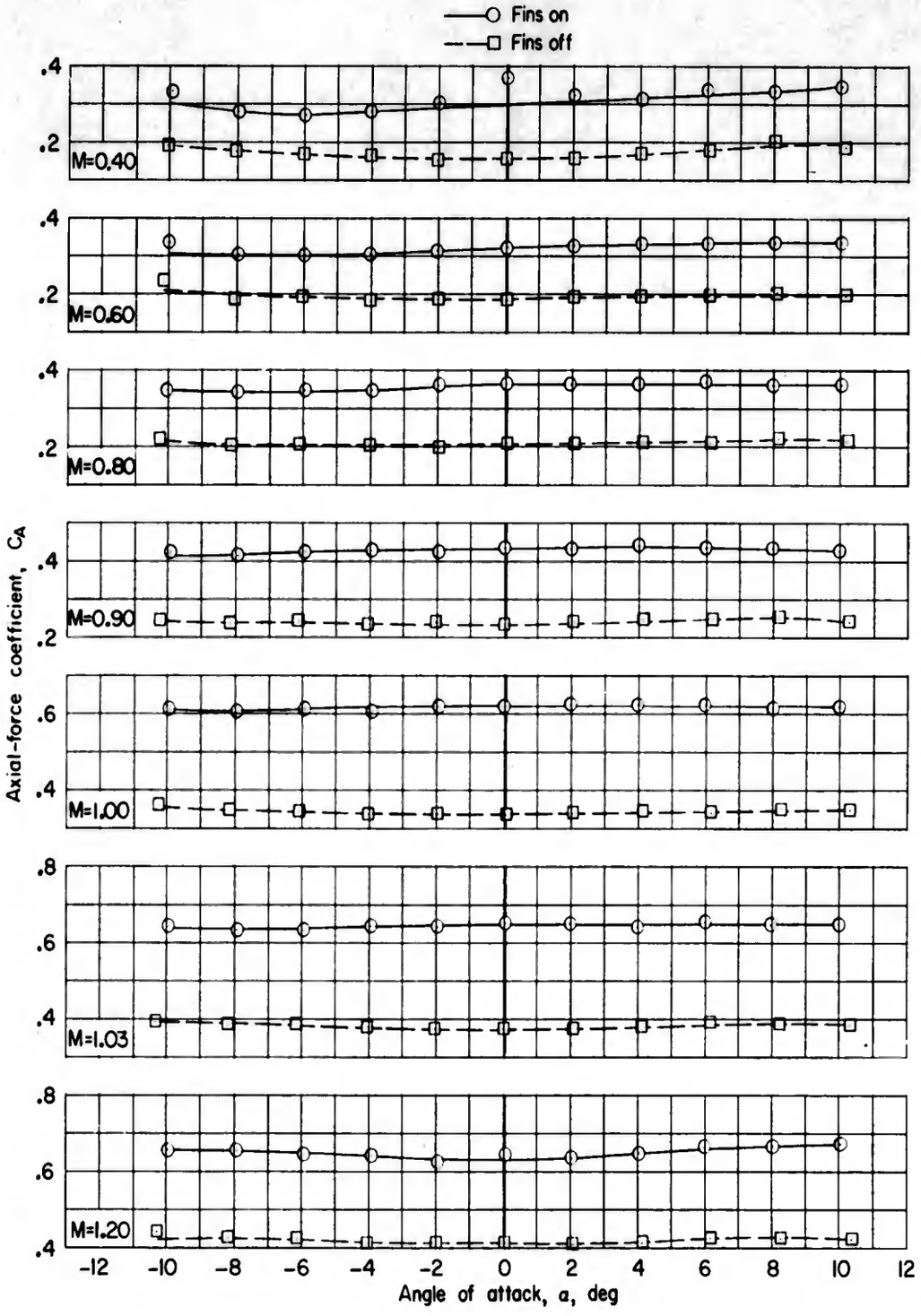

(d) C_A plotted against α; 8.2° flare half-angle.

Figure 6.- Continued.

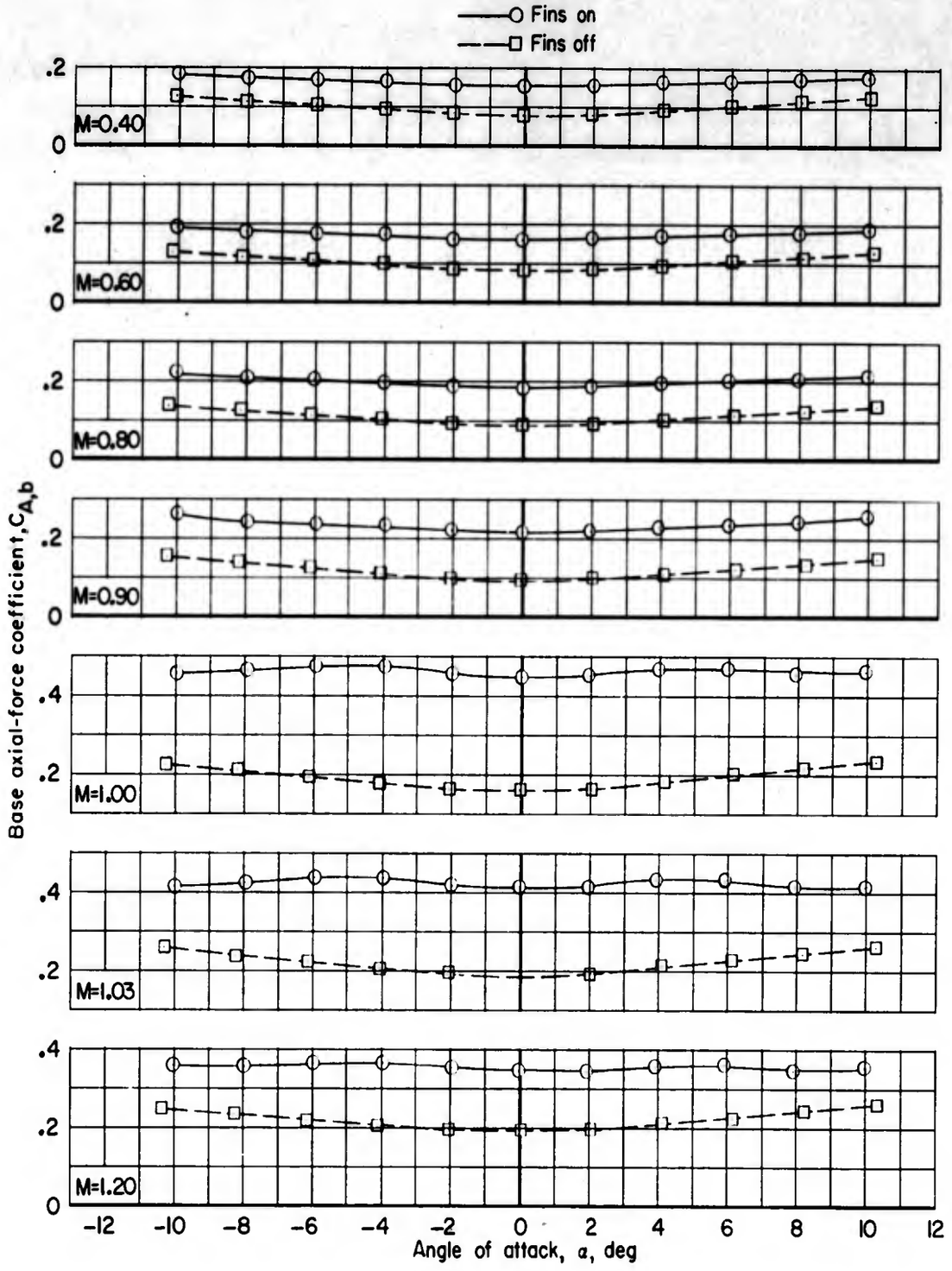

(e) $C_{A,b}$ plotted against α; 5.2° flare half-angle.

Figure 6.- Continued.

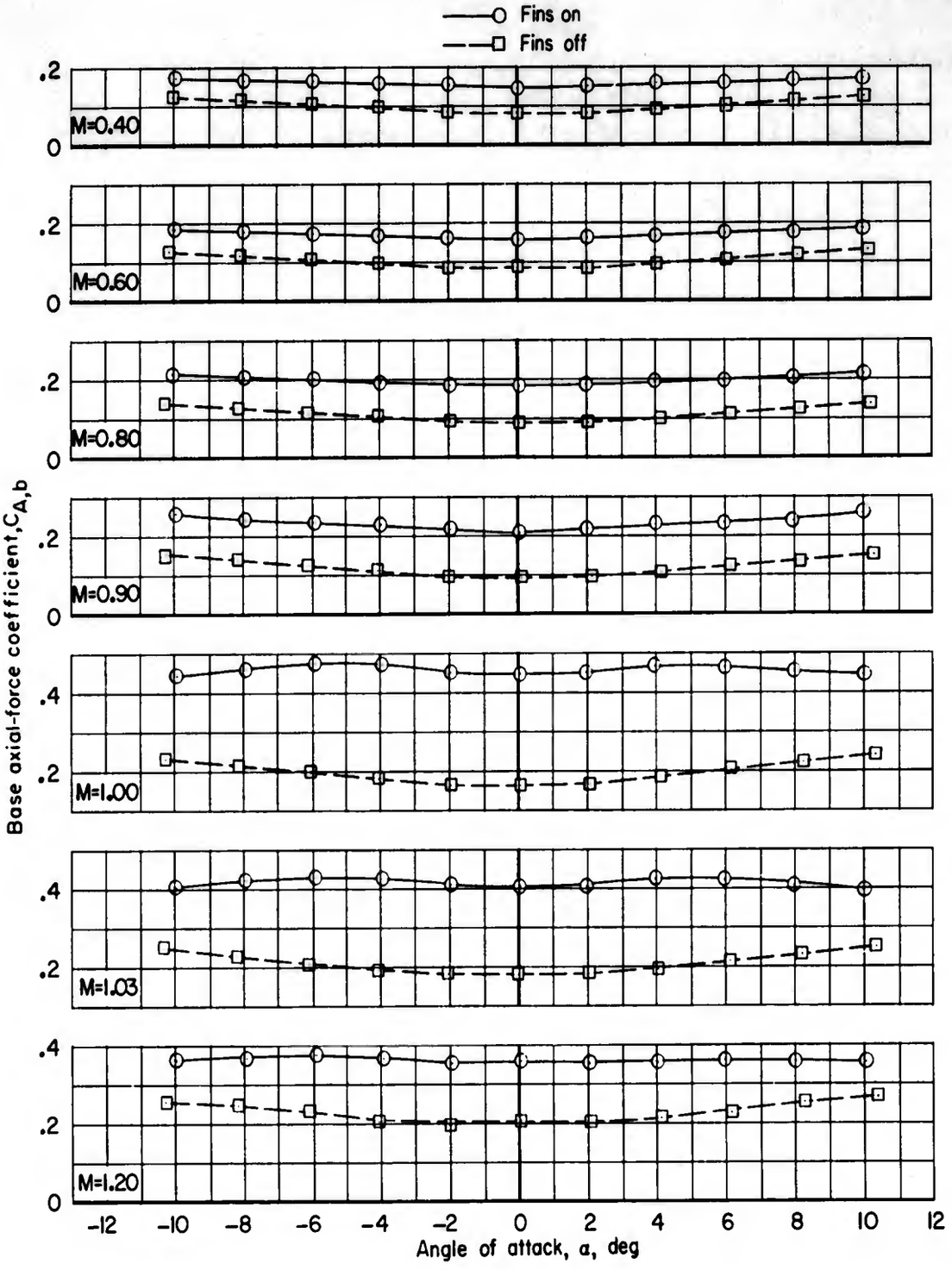

(f) $C_{A,b}$ plotted against α; 8.2° flare half-angle.

Figure 6.- Continued.

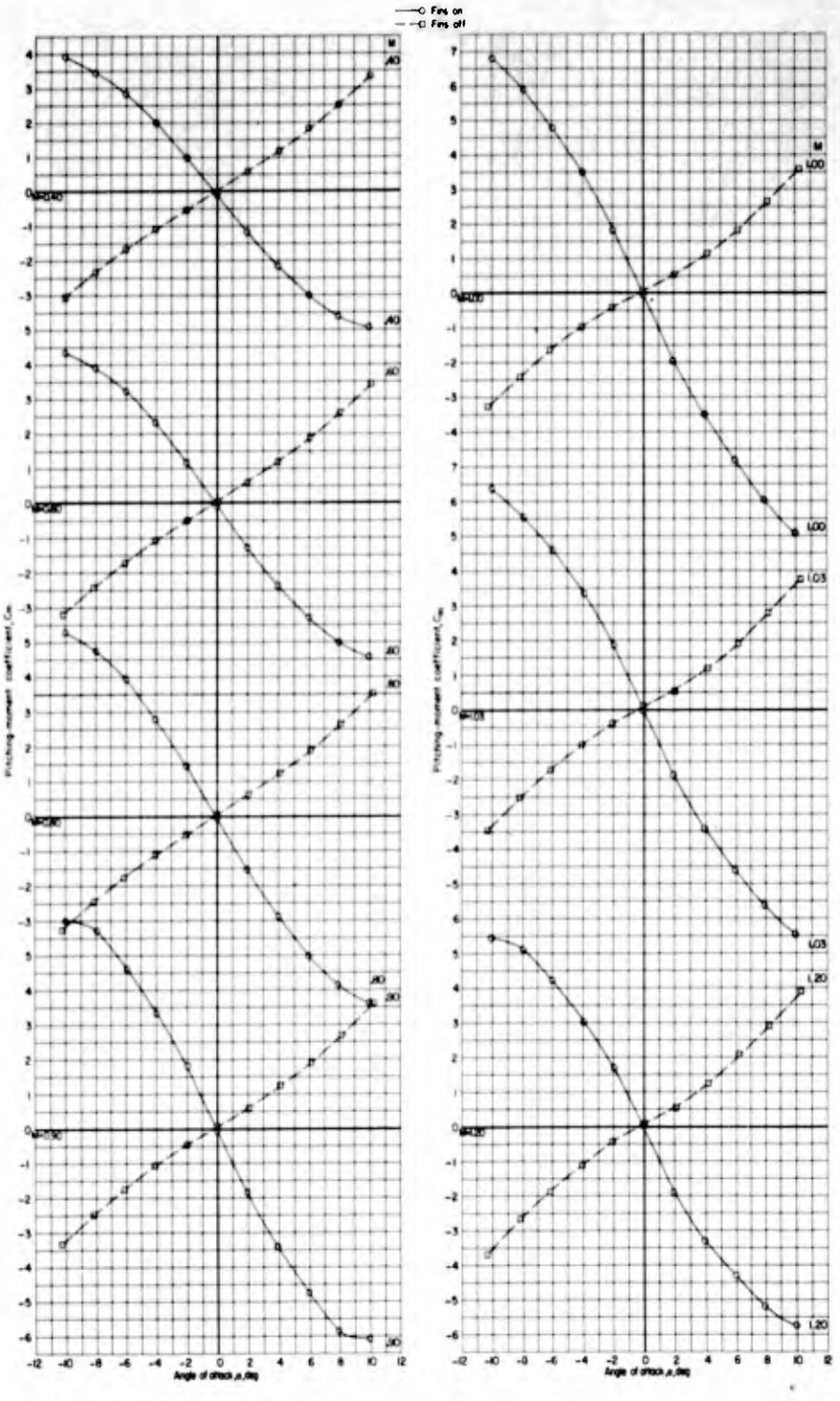

(g) C_m plotted against α; 5.2° flare half-angle.

Figure 6.- Continued.

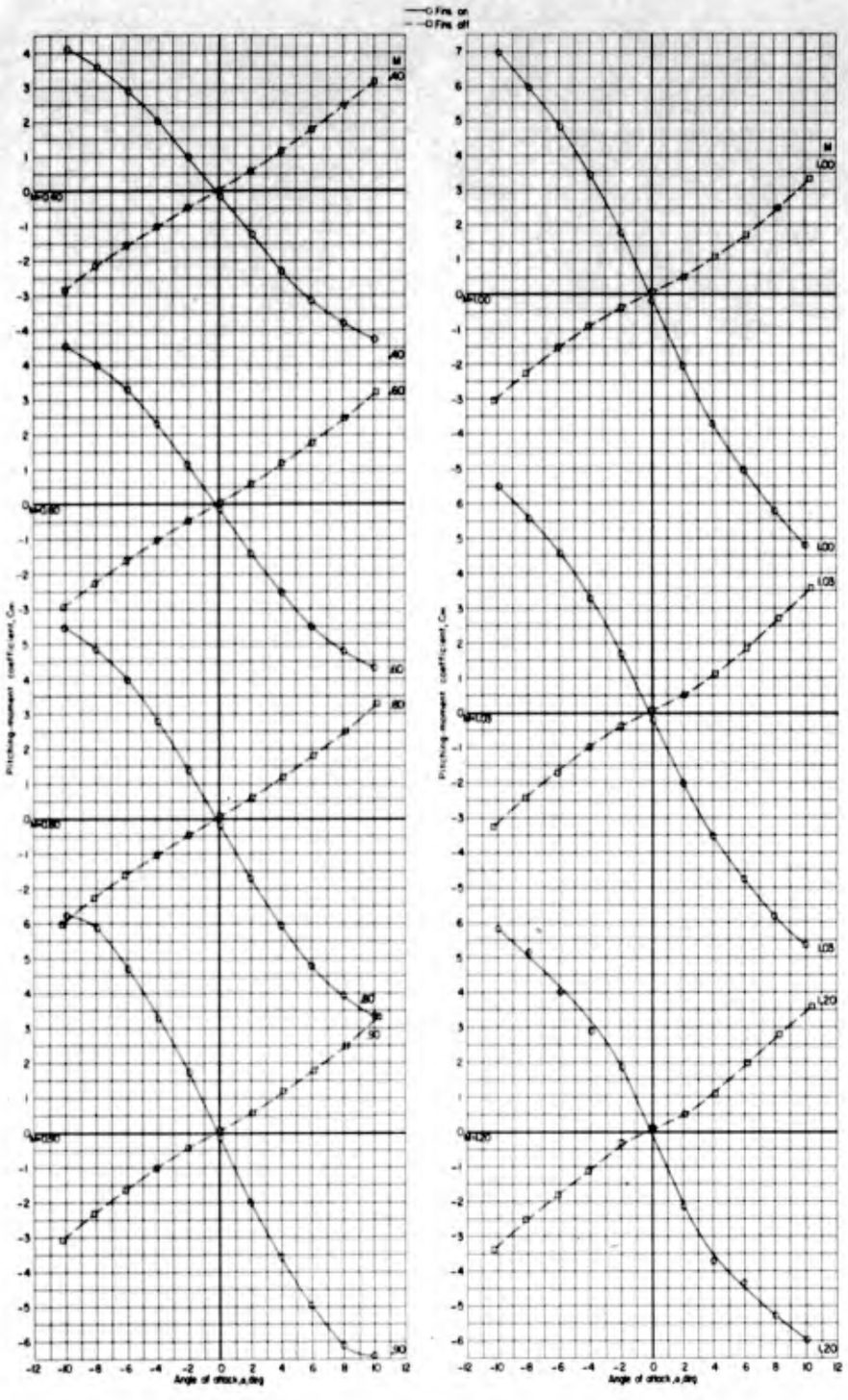

(h) C_m plotted against α; 8.2° flare half-angle.

Figure 6.- Continued.

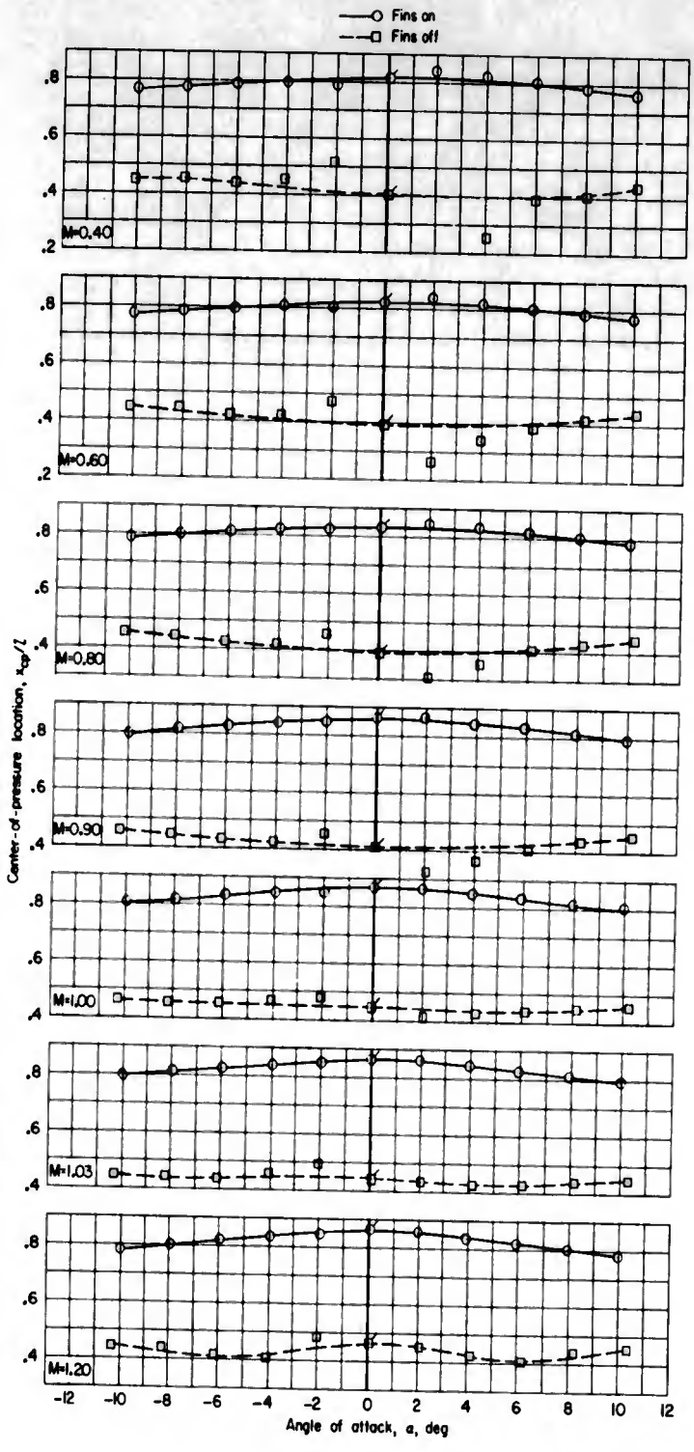

(i) $\frac{x_{cp}}{l}$ plotted against α; 5.2° flare half-angle.

Figure 6.- Continued.

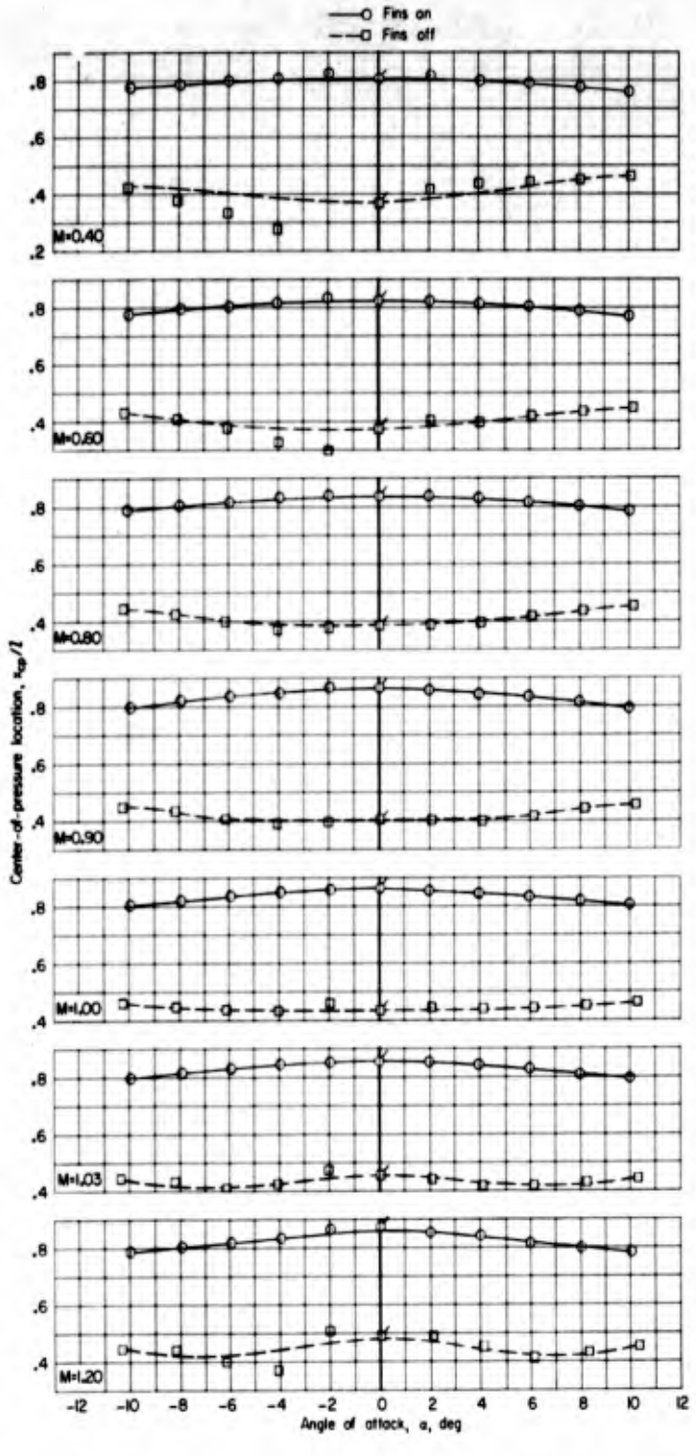

(j) $\frac{x_{cp}}{l}$ plotted against α; 8.2° flare half-angle.

Figure 6.- Concluded.

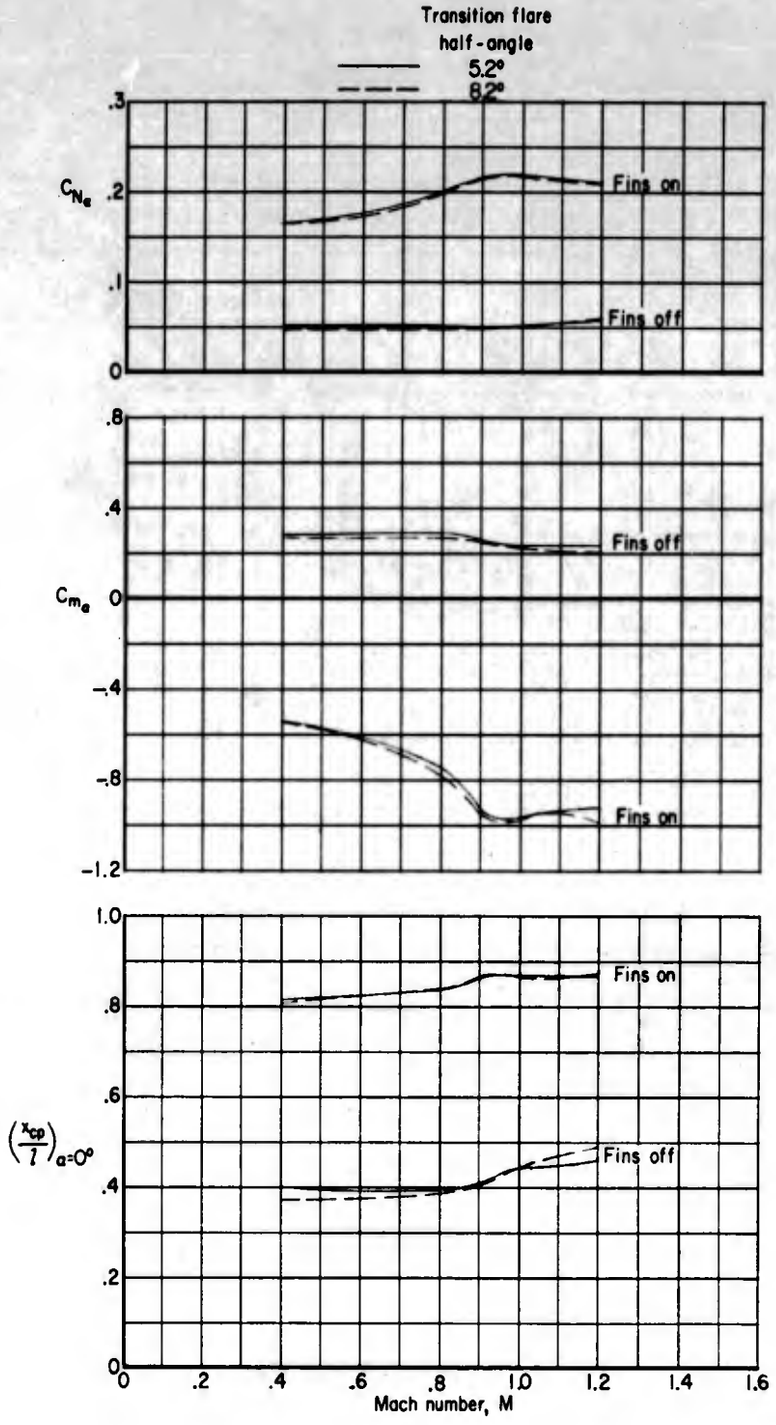

(a) C_{N_α}, C_{m_α}, and $\frac{x_{cp}}{l}$ plotted against Mach number. $\alpha = 0°$.

Figure 7.- Summary of aerodynamic characteristics in pitch. 1/15-scale four-stage research model.

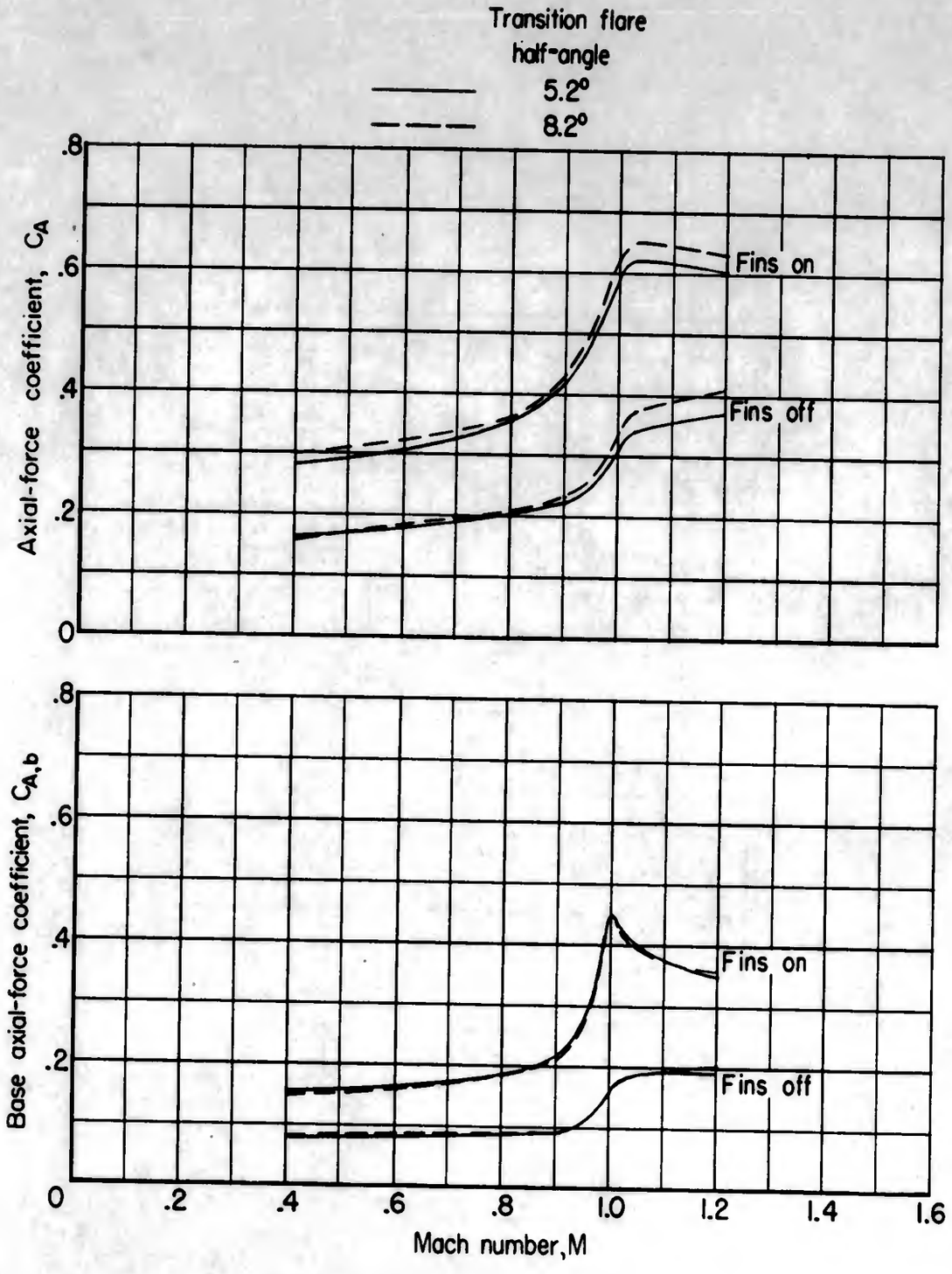

(b) C_A and $C_{A,b}$ plotted against Mach number. $\alpha = 0°$.

Figure 7.- Concluded.

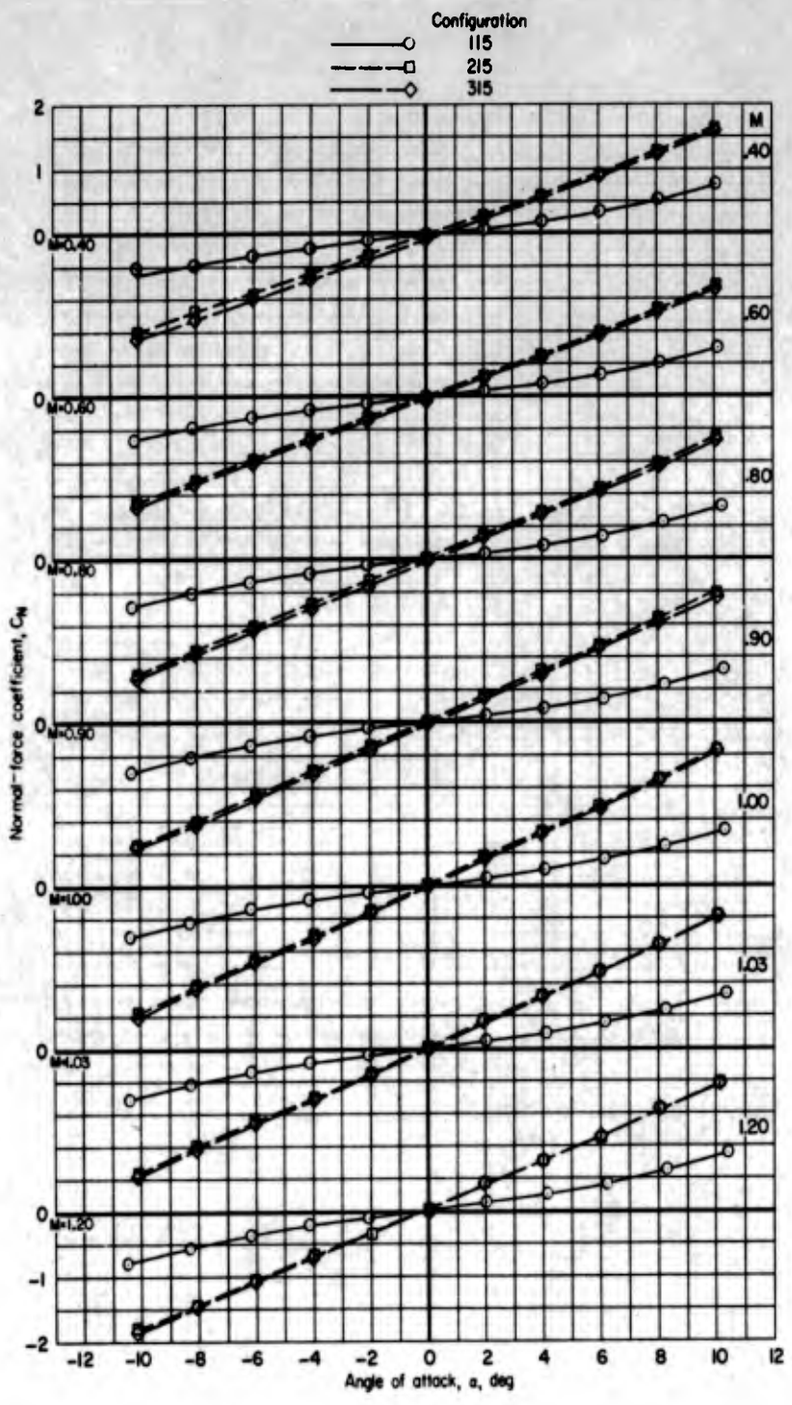

(a) C_N plotted against α.

Figure 8.- Effects of delta fins and protuberances on aerodynamic characteristics in pitch. Configurations of 1/15-scale four-stage Scout model.

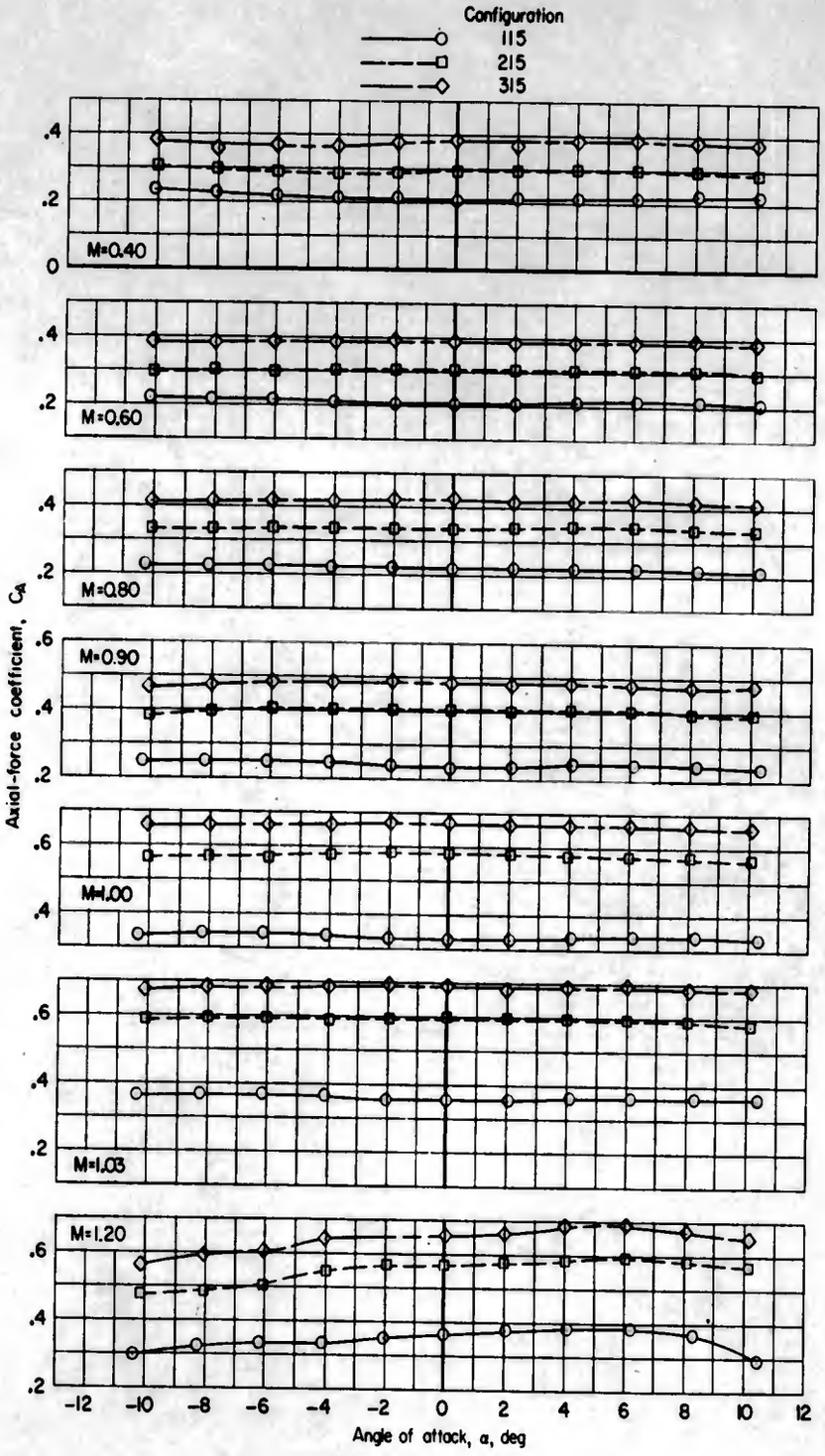

(b) C_A plotted against α.

Figure 8.- Continued.

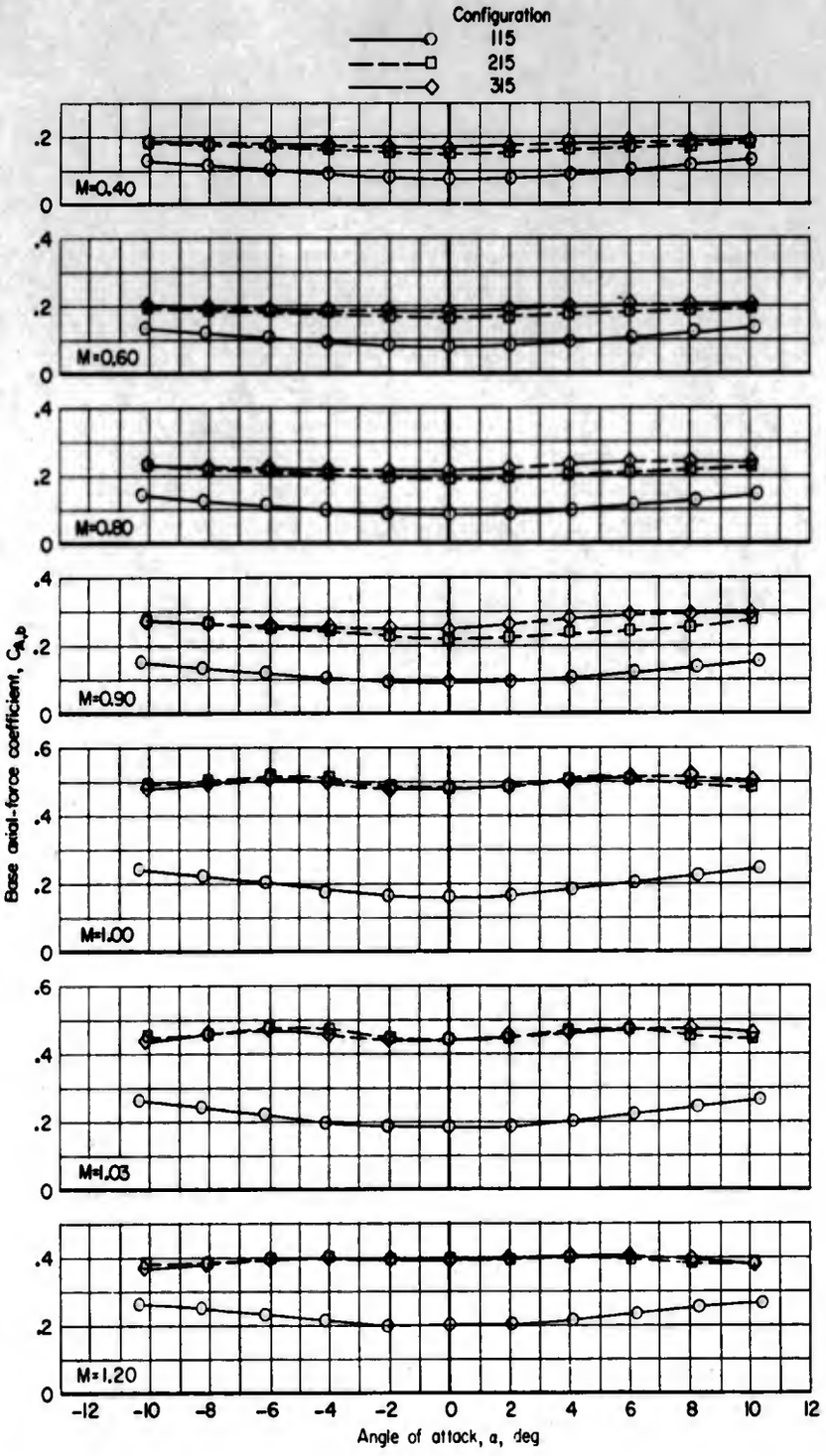

(c) $C_{A,b}$ plotted against α.

Figure 8.- Continued.

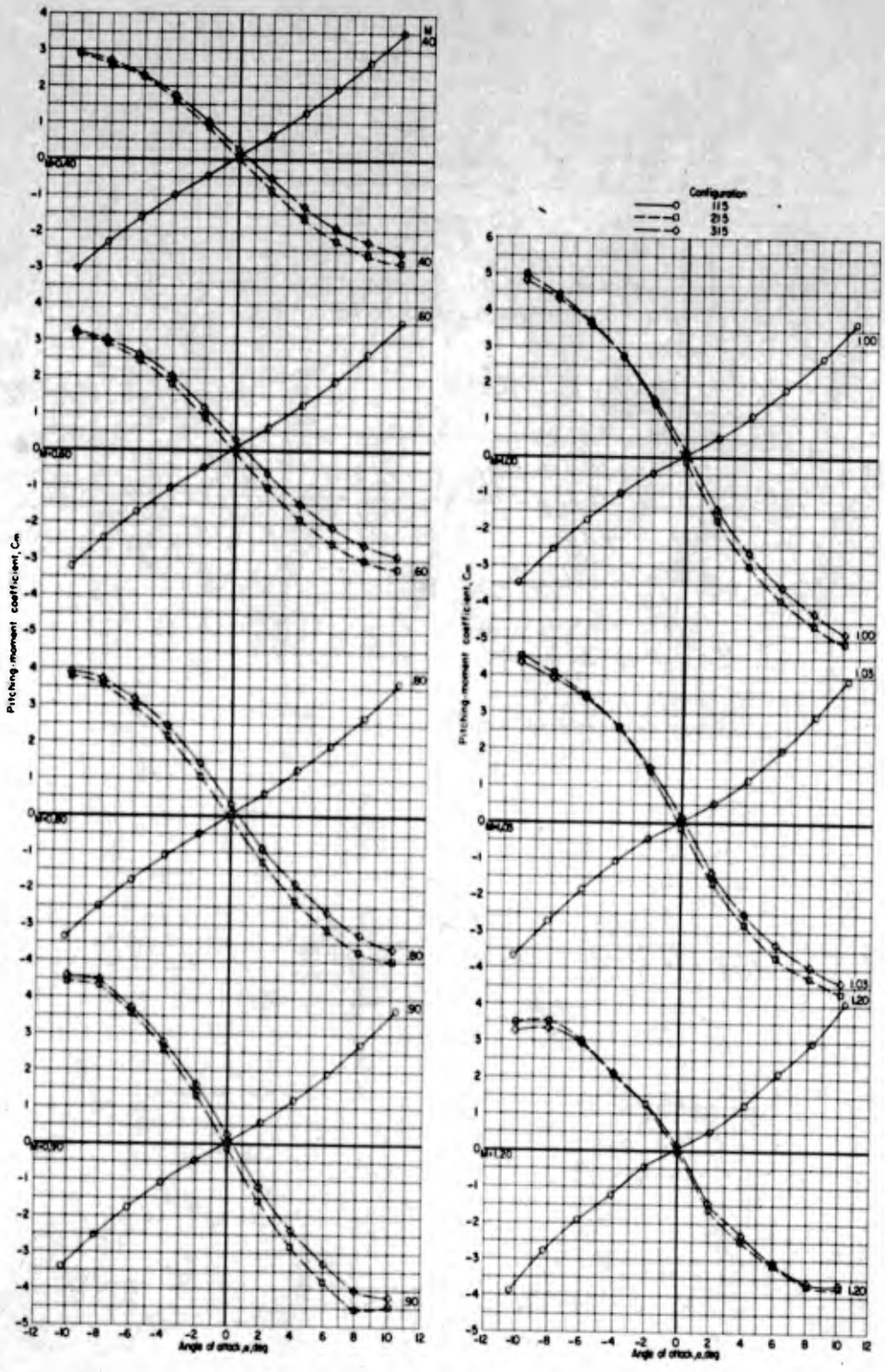

(d) C_m plotted against α.

Figure 8.- Continued.

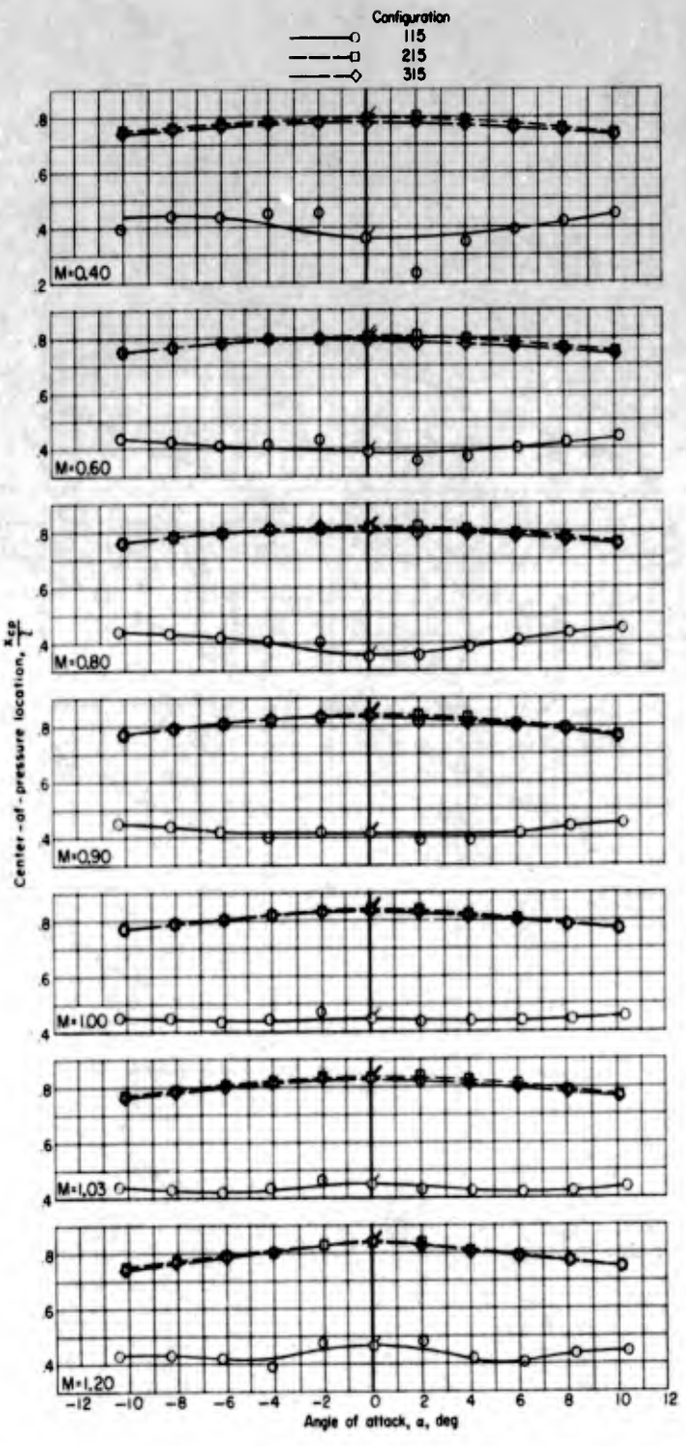

(e) $\frac{x_{cp}}{l}$ plotted against α.

Figure 8.- Concluded.

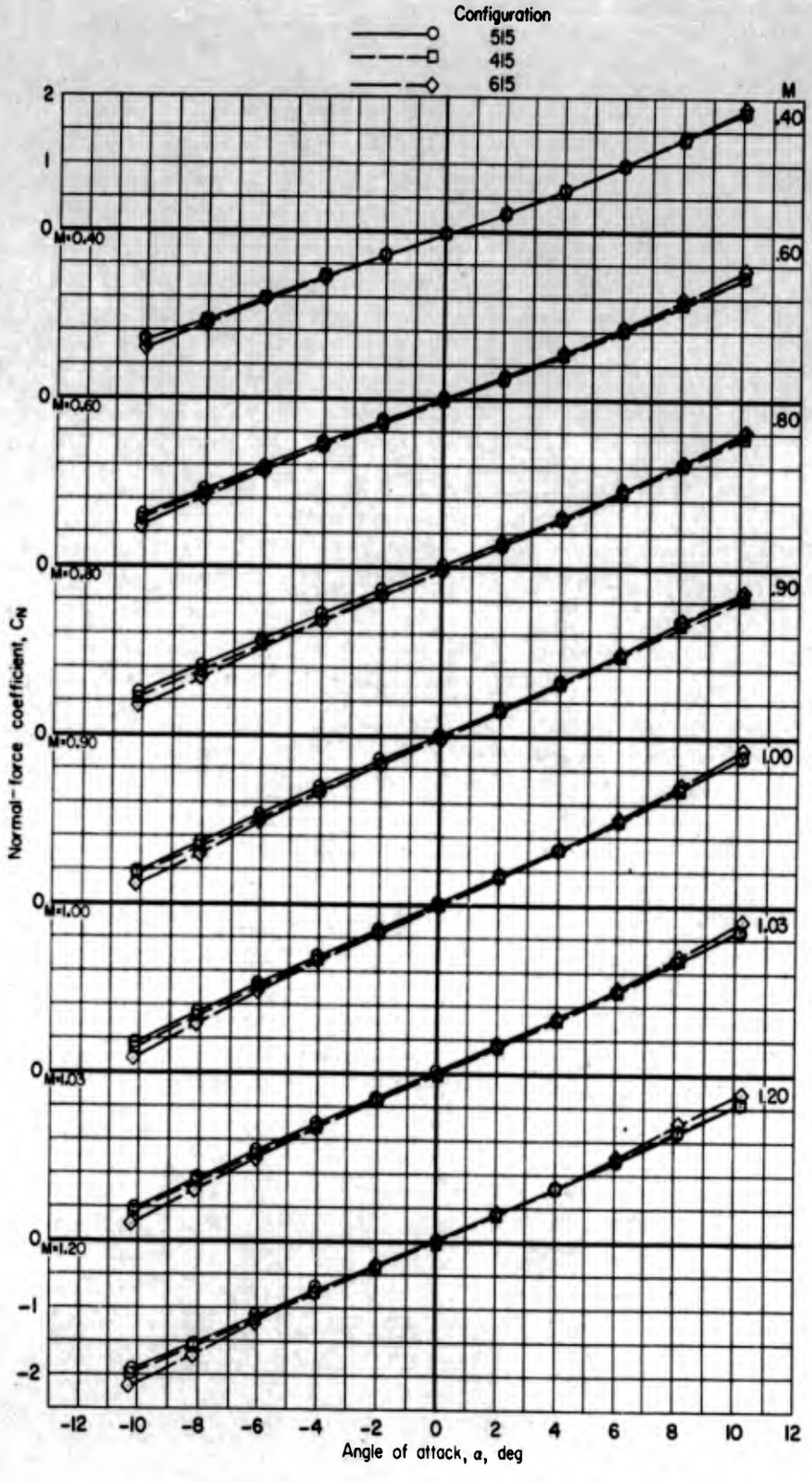

(a) C_N plotted against α.

Figure 9.- Effects of stub-fin orientation and protuberances on aerodynamic characteristics in pitch. Configurations of 1/15-scale four-stage Scout model.

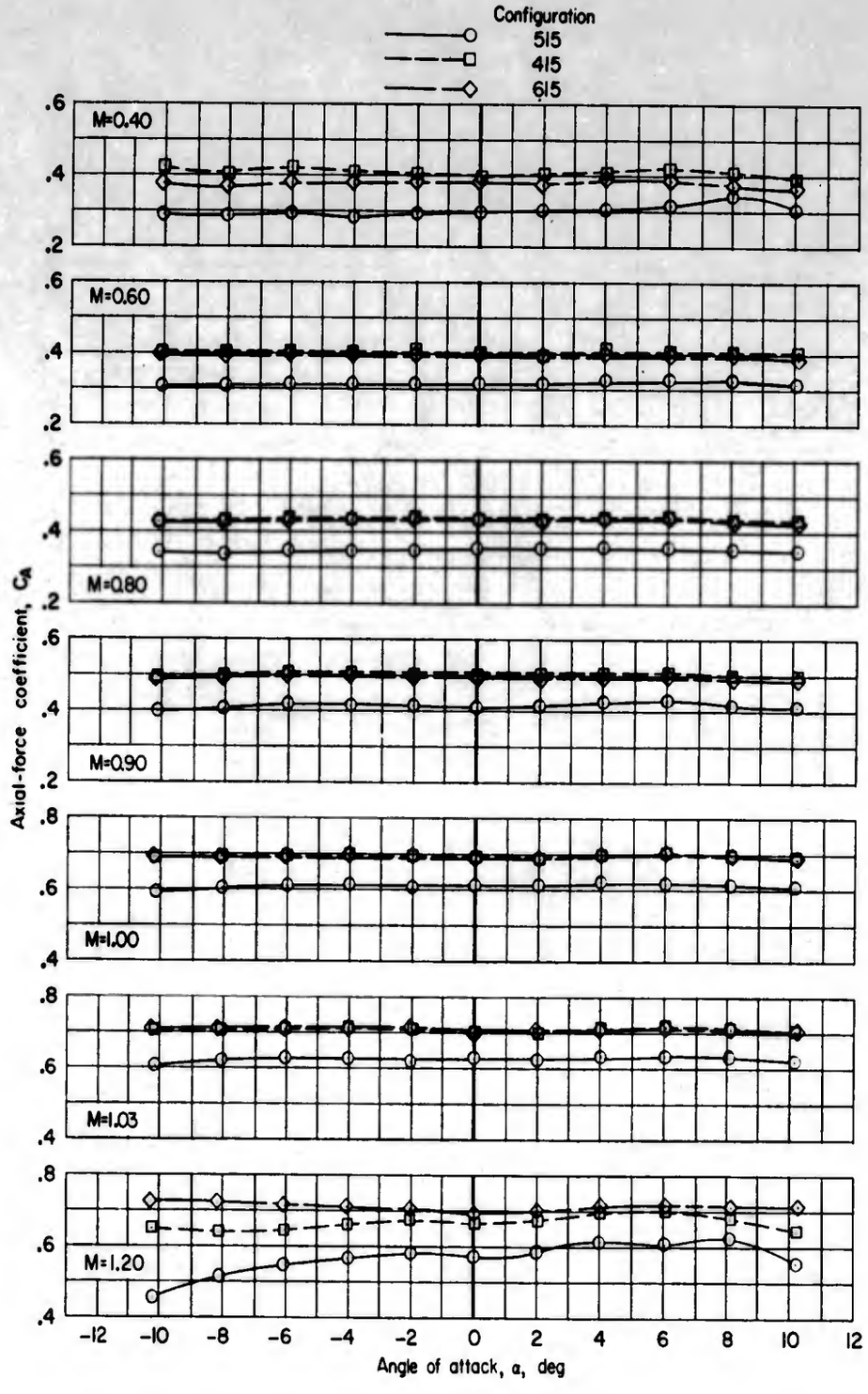

(b) C_A plotted against α.

Figure 9.- Continued.

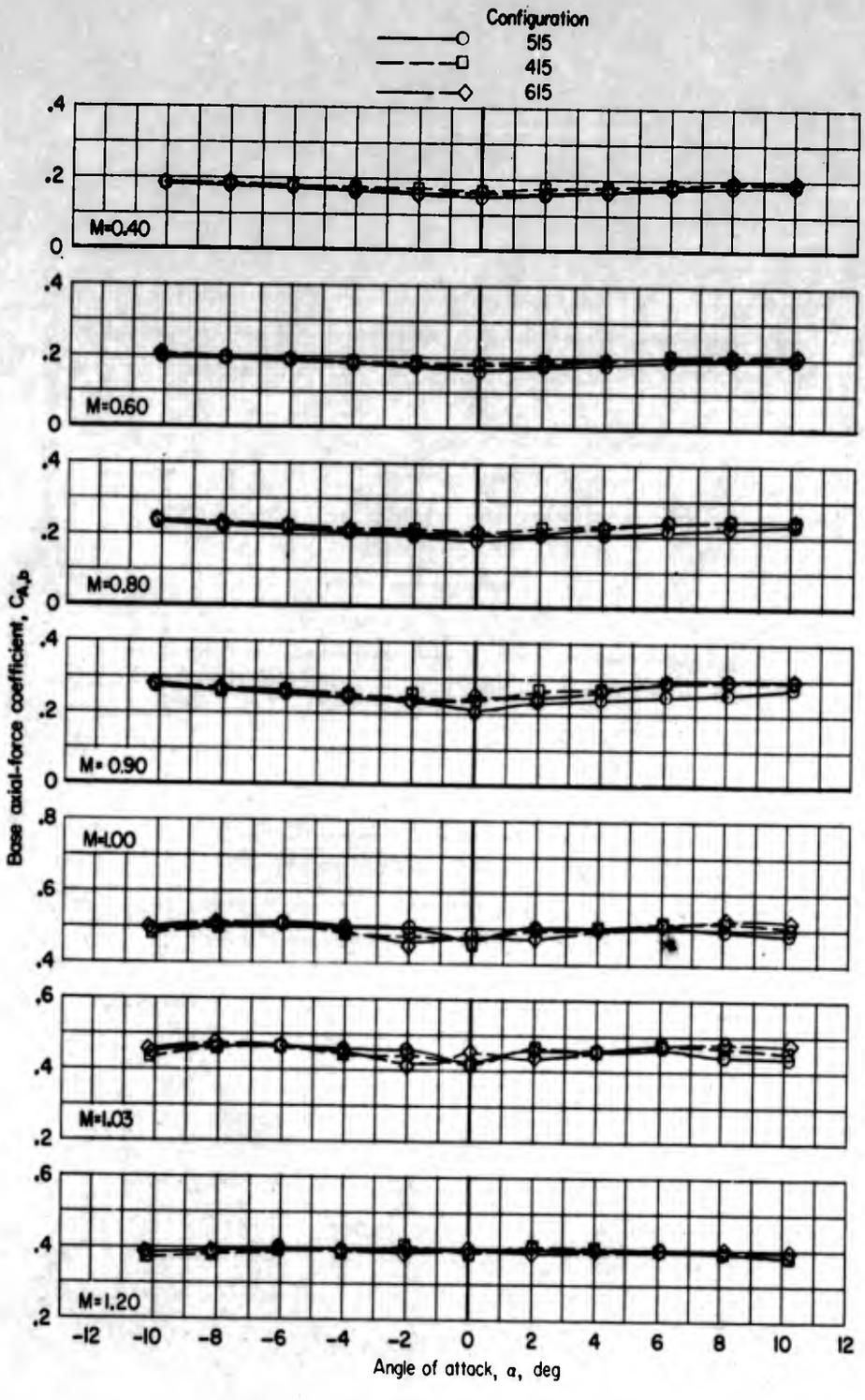

(c) $C_{A,b}$ plotted against α.

Figure 9.- Continued.

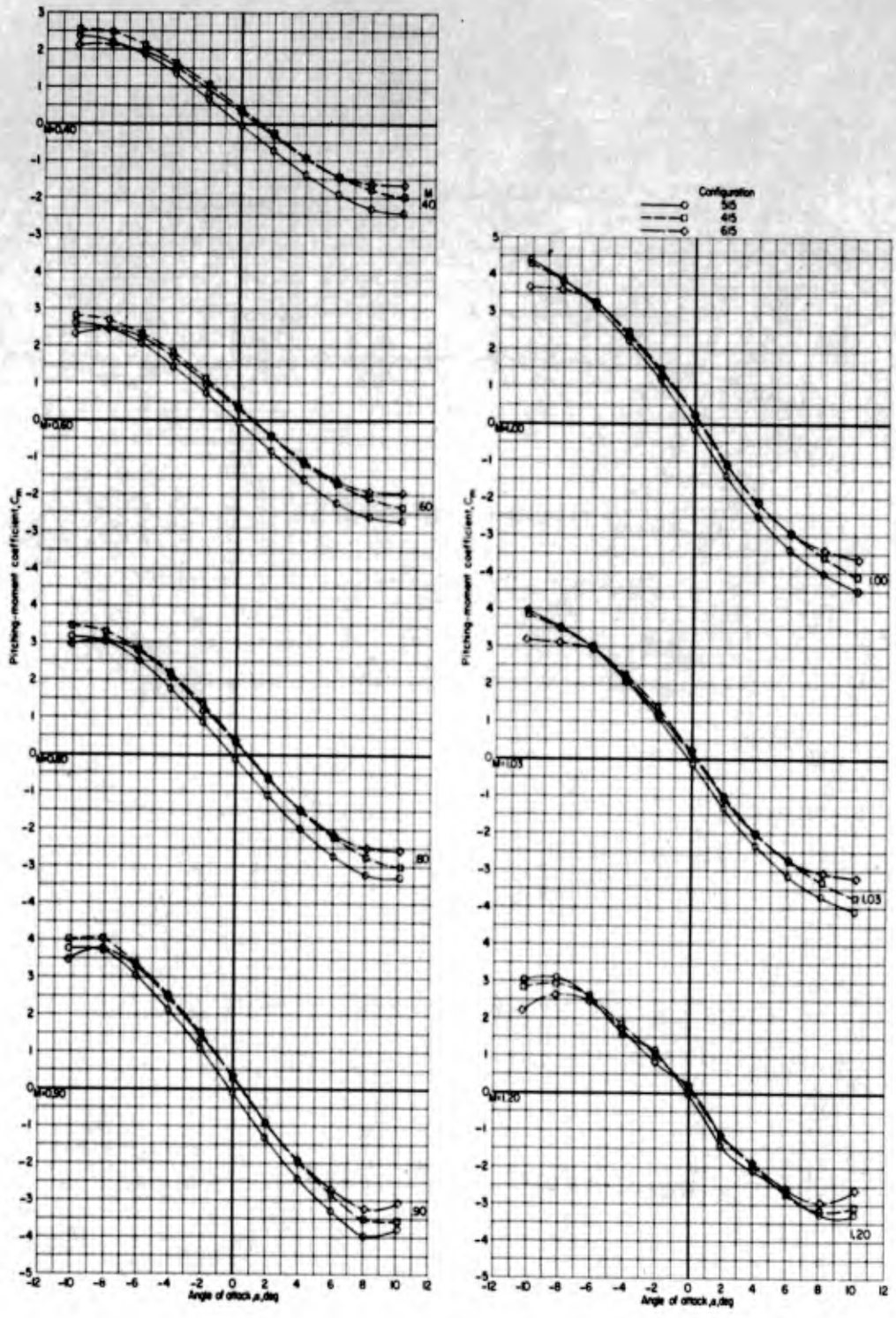

(d) C_m plotted against α.

Figure 9.- Continued.

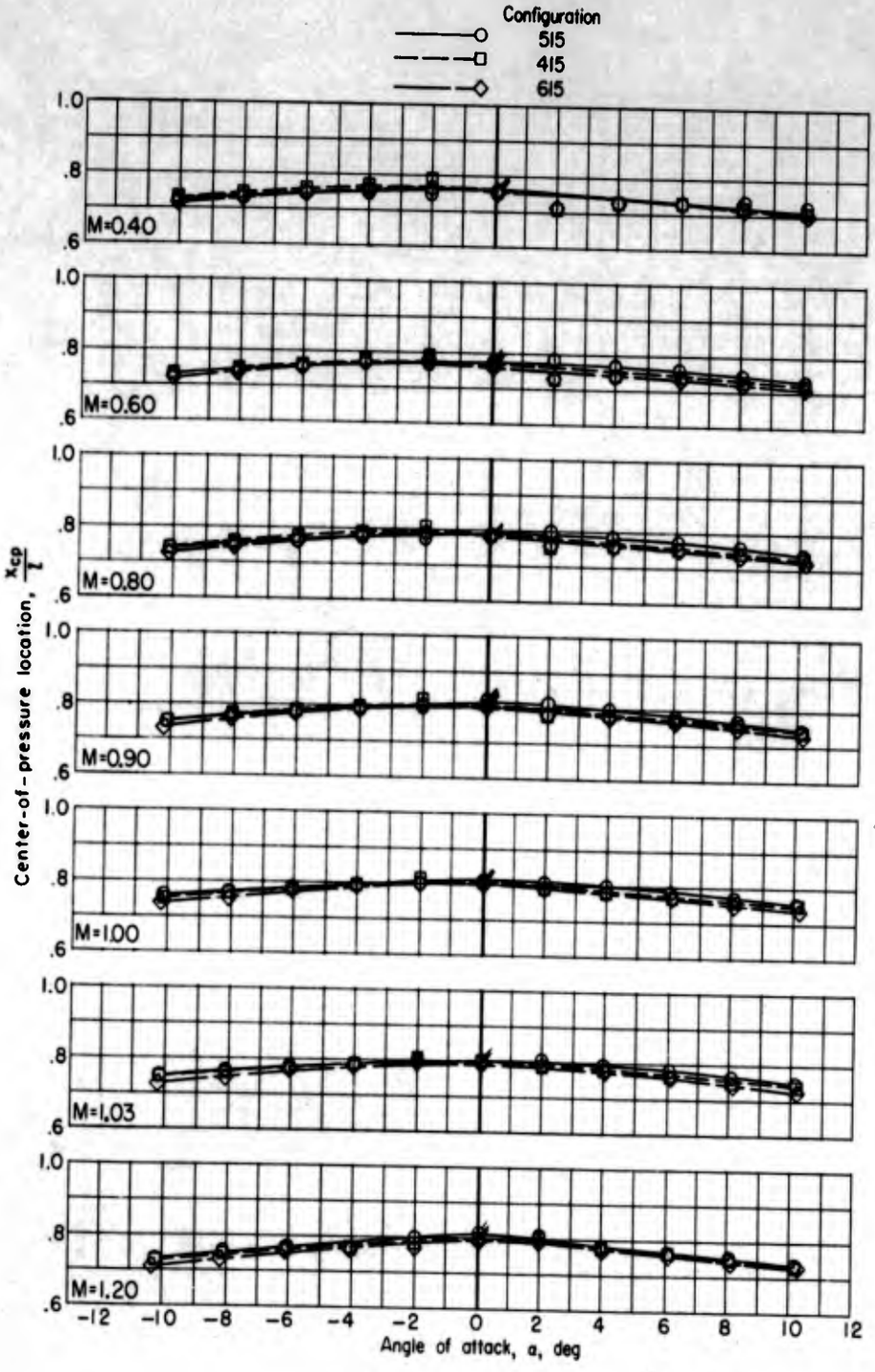

(e) $\frac{x_{cp}}{l}$ plotted against α.

Figure 9.- Concluded.

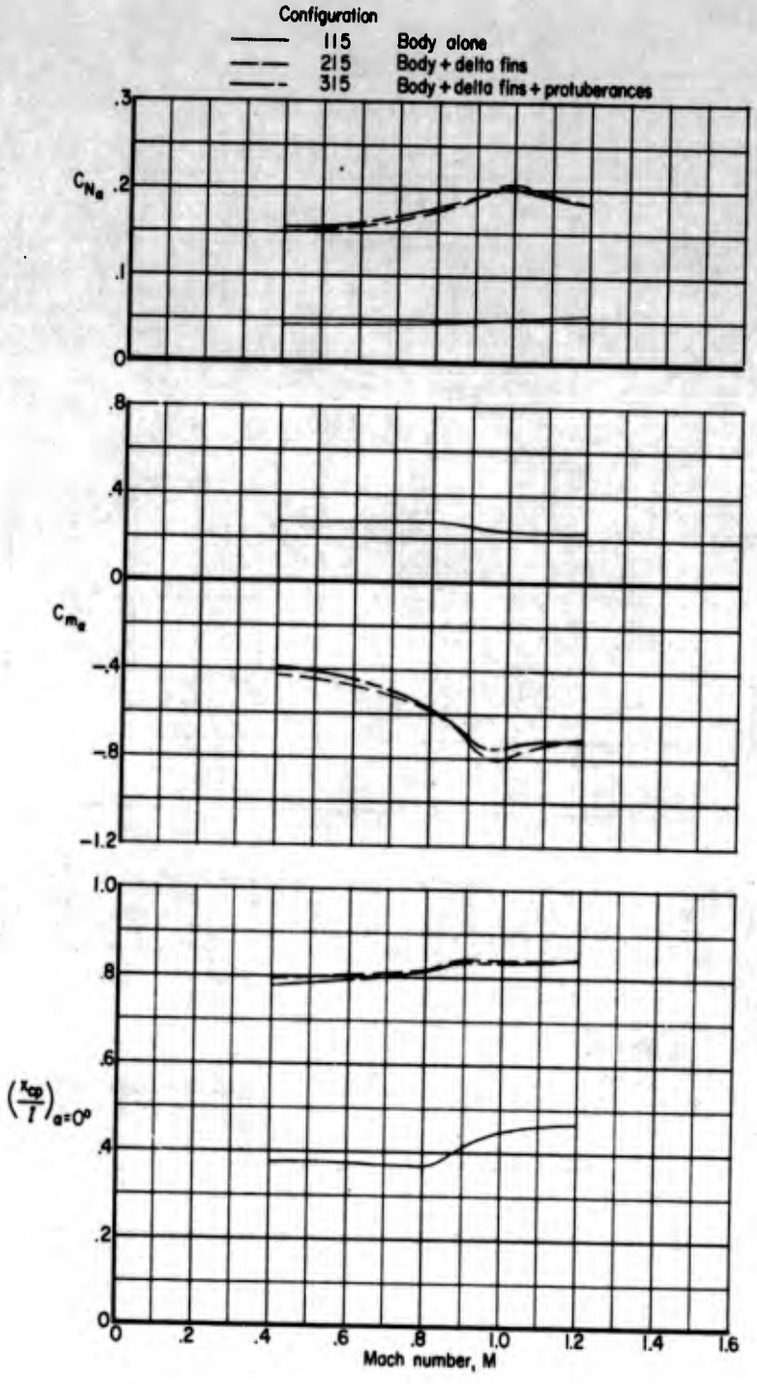

(a) C_{N_α}, C_{m_α}, and $\frac{x_{cp}}{l}$ plotted against Mach number. $\alpha = 0^\circ$.

Figure 10.- Summary of effects of delta fins and protuberances on aerodynamic characteristics in pitch. Configurations of 1/15-scale four-stage Scout model.

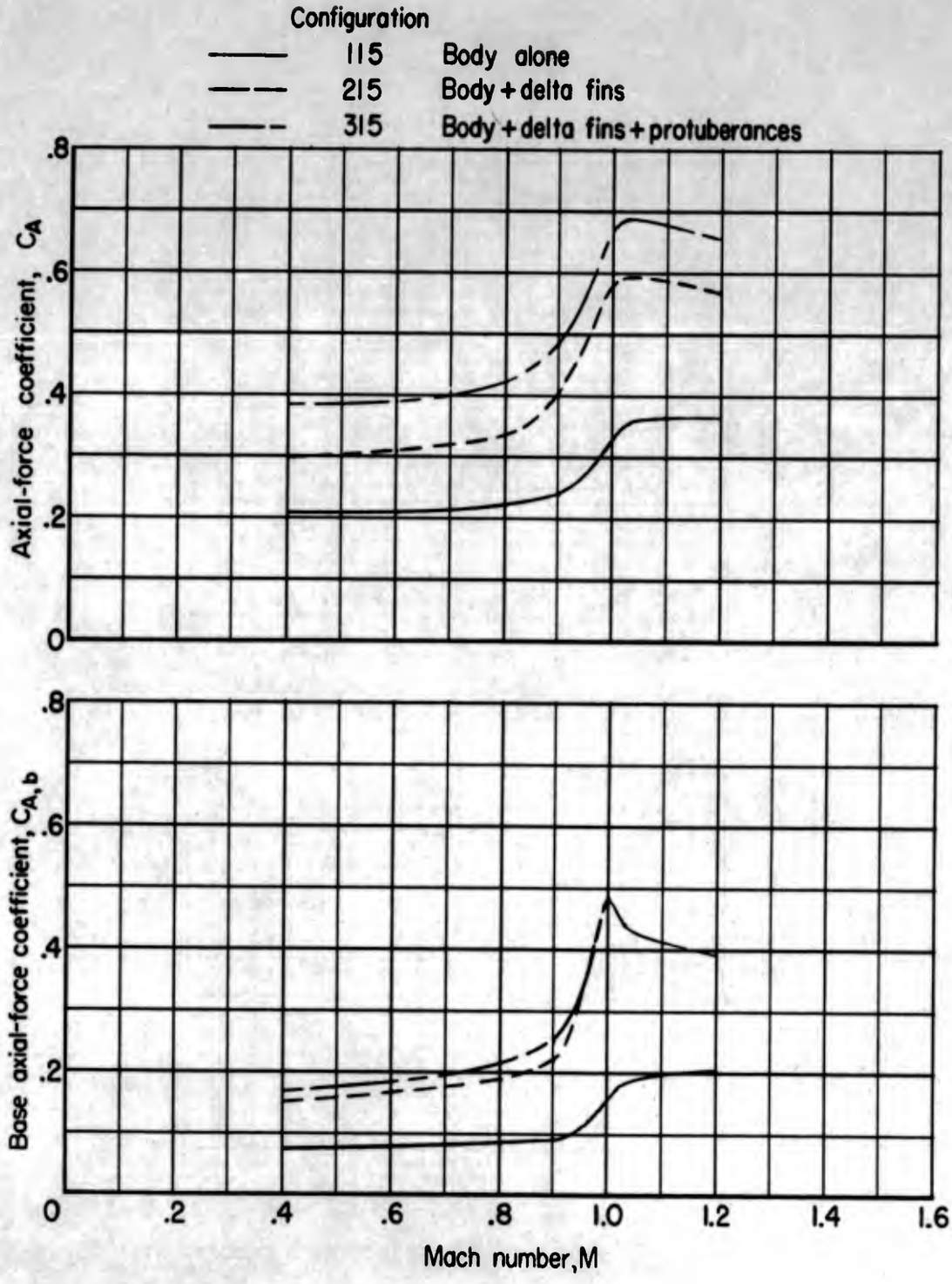

(b) C_A and $C_{A,b}$ plotted against Mach number. $\alpha = 0^\circ$.

Figure 10.- Concluded.

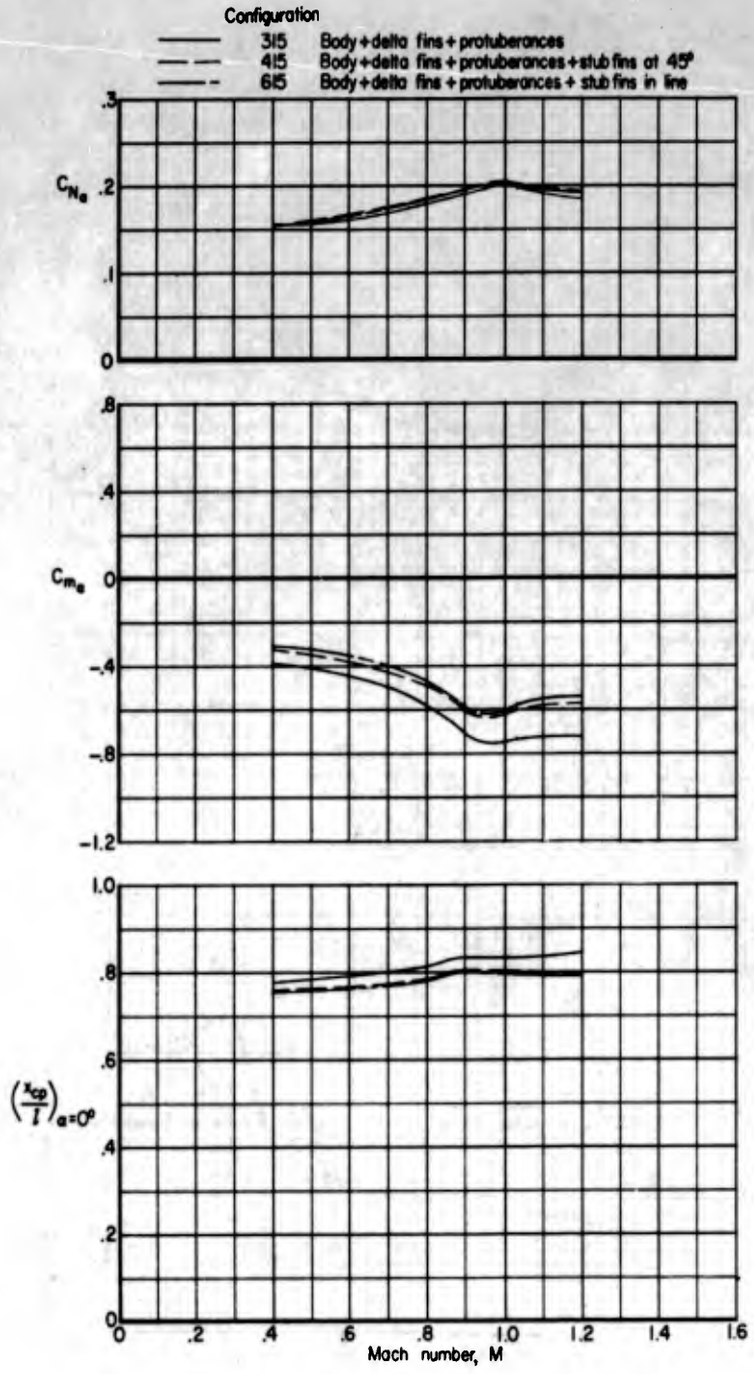

(a) C_{N_α}, C_{m_α}, and $\frac{x_{cp}}{l}$ plotted against Mach number. $\alpha = 0°$.

Figure 11.- Summary of effects of added stub fins and stub-fin orientation on aerodynamic characteristics in pitch. Configurations of 1/15-scale four-stage Scout model.

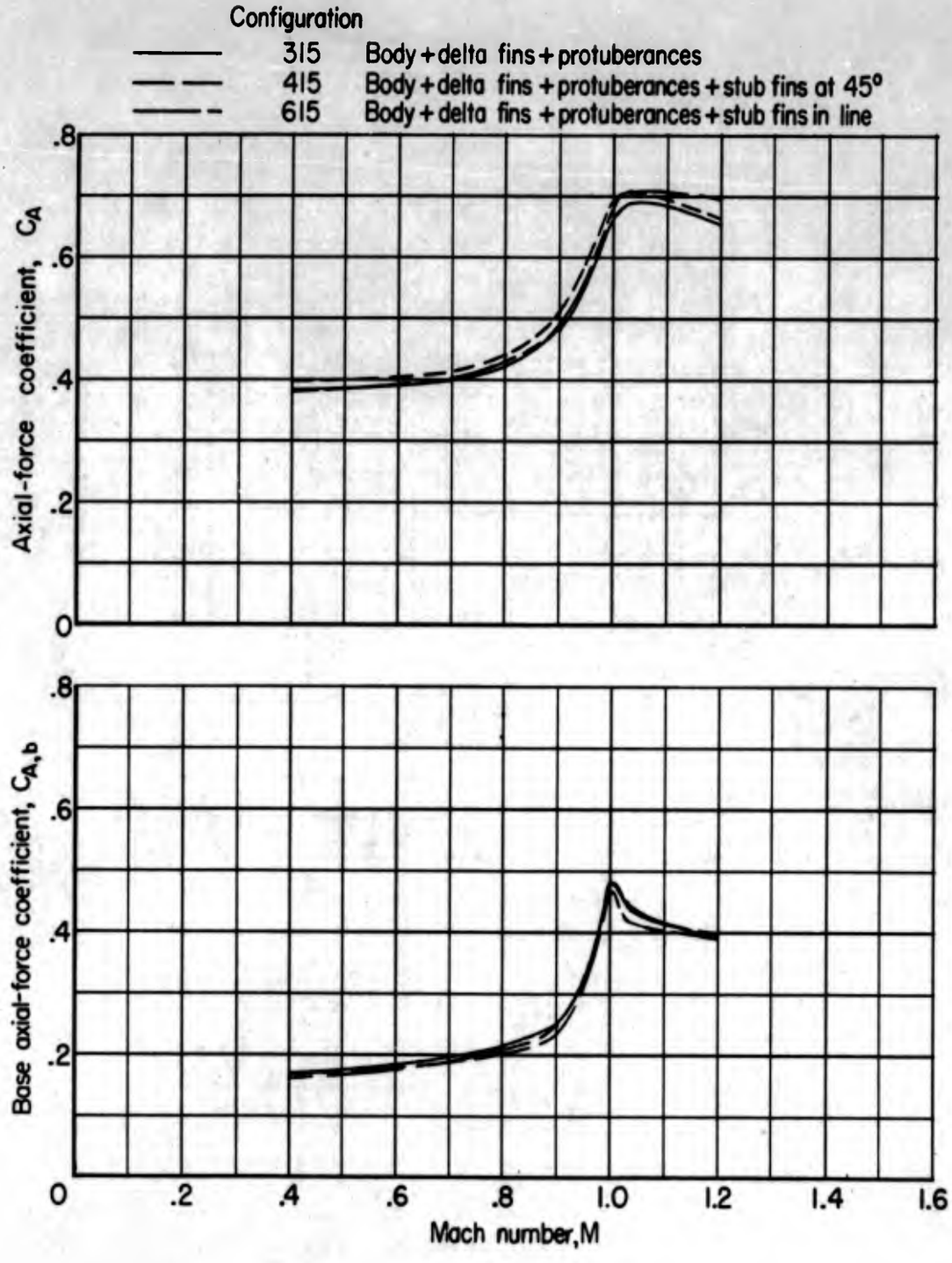

(b) C_A and $C_{A,b}$ plotted against Mach number. $\alpha = 0°$.

Figure 11.- Concluded.

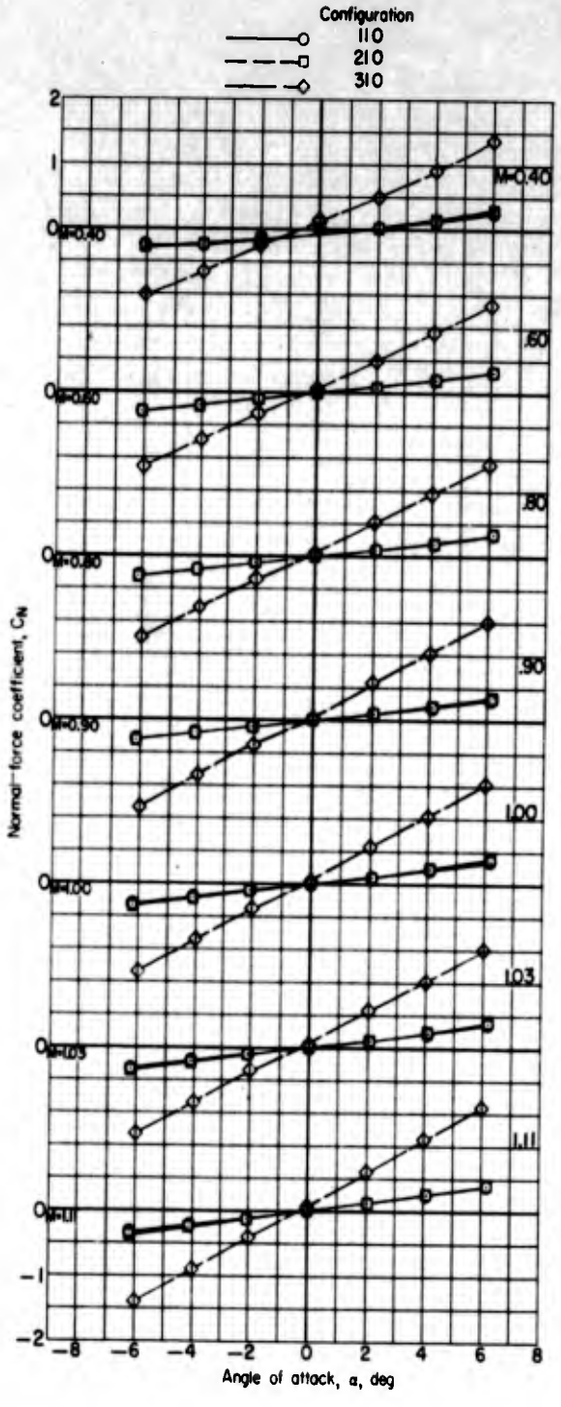

(a) C_N plotted against α.

Figure 12.- Effects of delta fins and protuberances on aerodynamic characteristics in pitch for configurations with cylindrical afterbody. 1/10-scale three-stage Scout model.

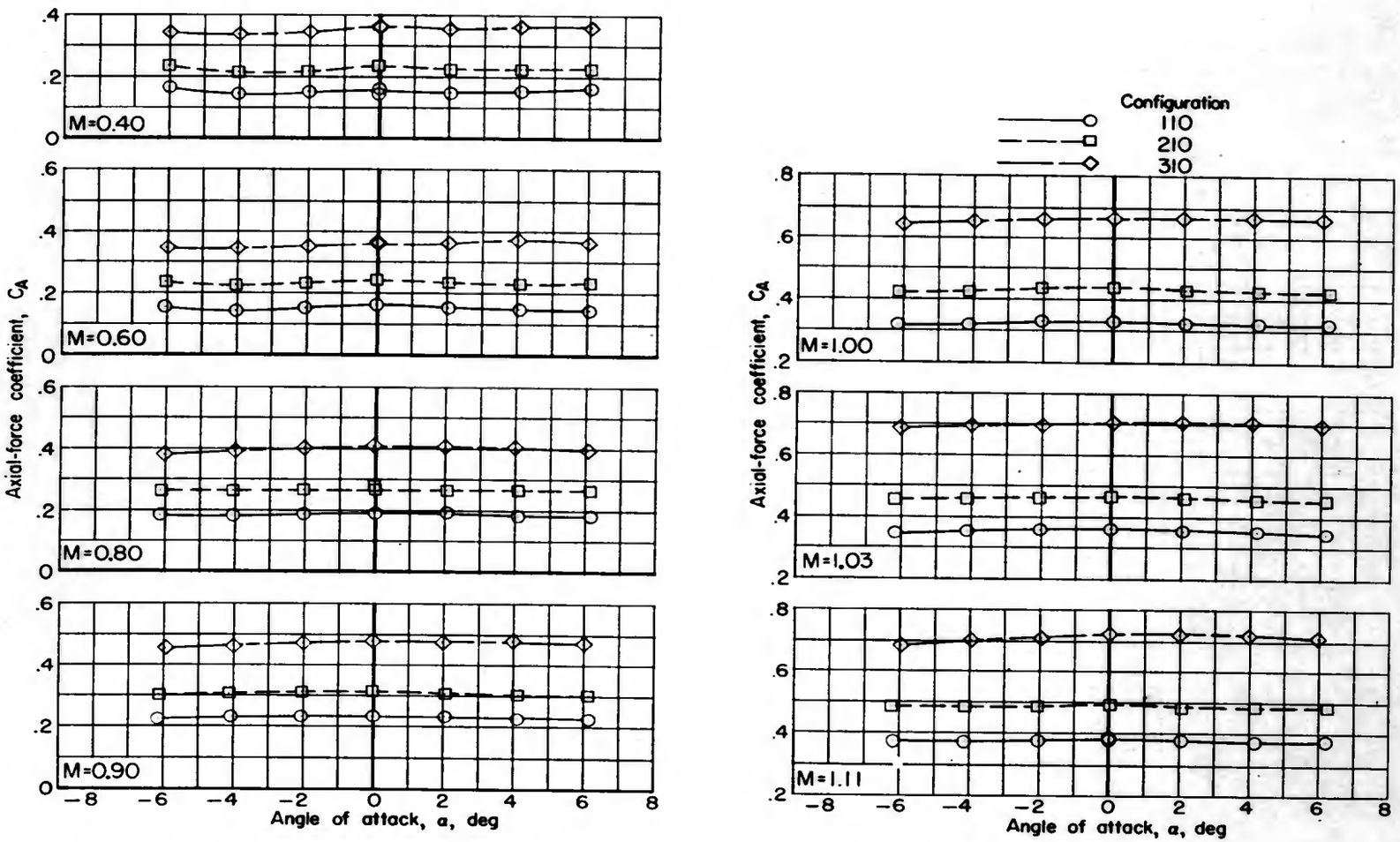

(b) C_A plotted against α.

Figure 12.- Continued.

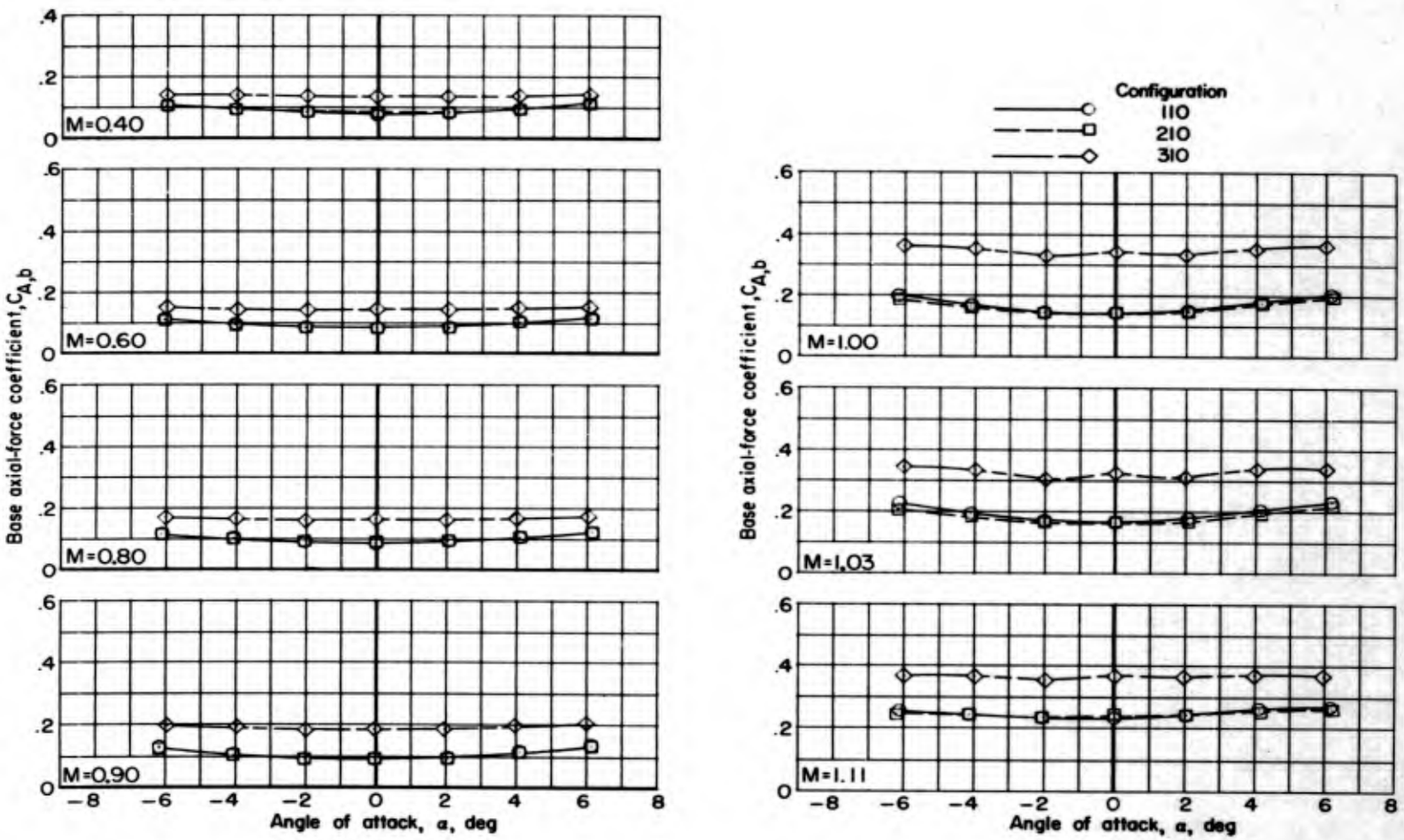

(c) $C_{A,b}$ plotted against α.

Figure 12.- Continued.

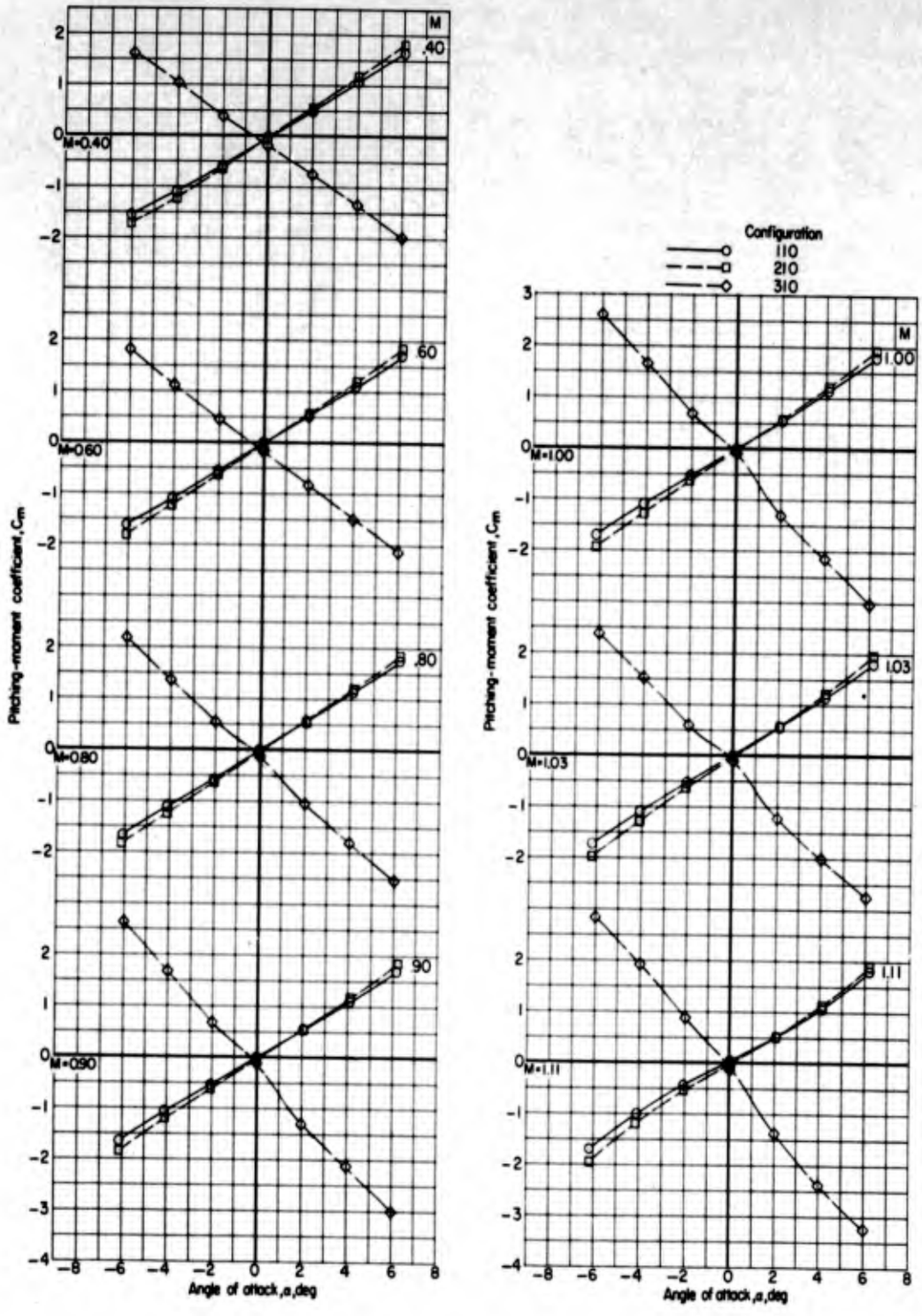

(d) C_m plotted against α.

Figure 12.- Continued.

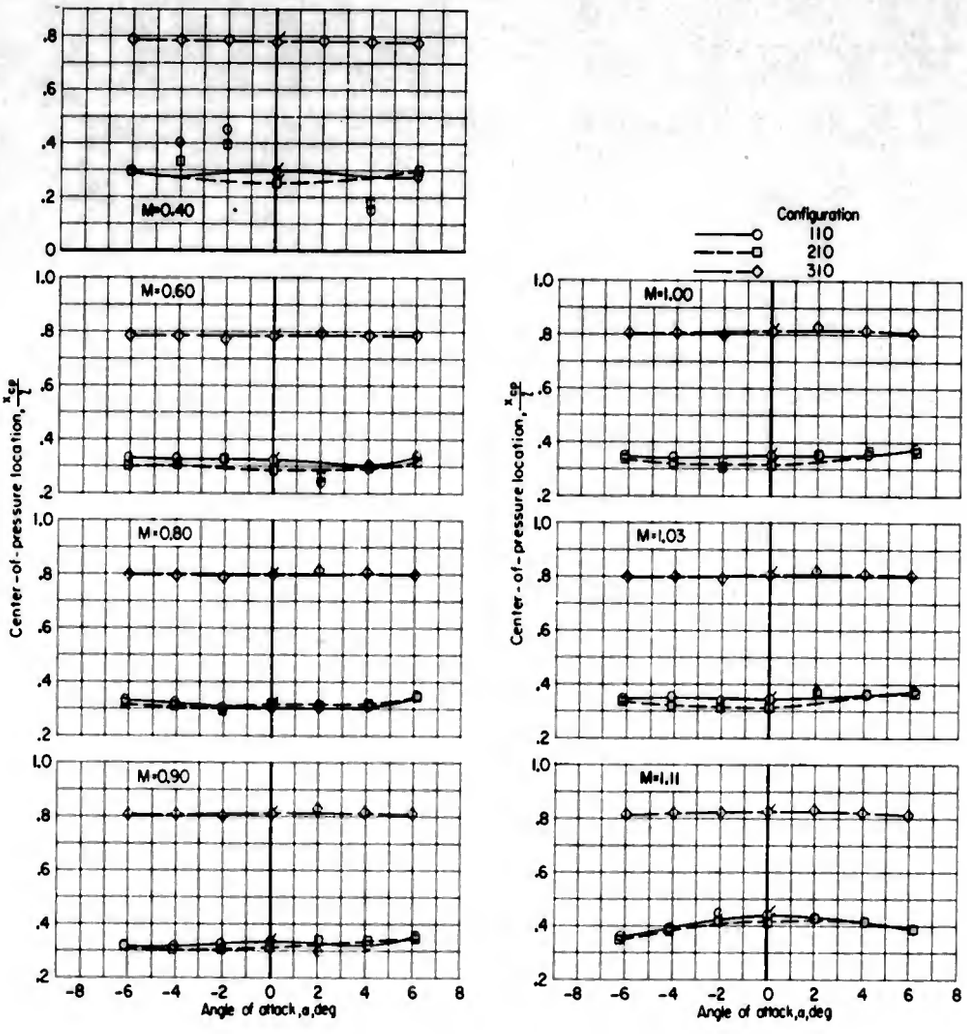

(e) $\frac{x_{cp}}{l}$ plotted against α.

Figure 12.- Concluded.

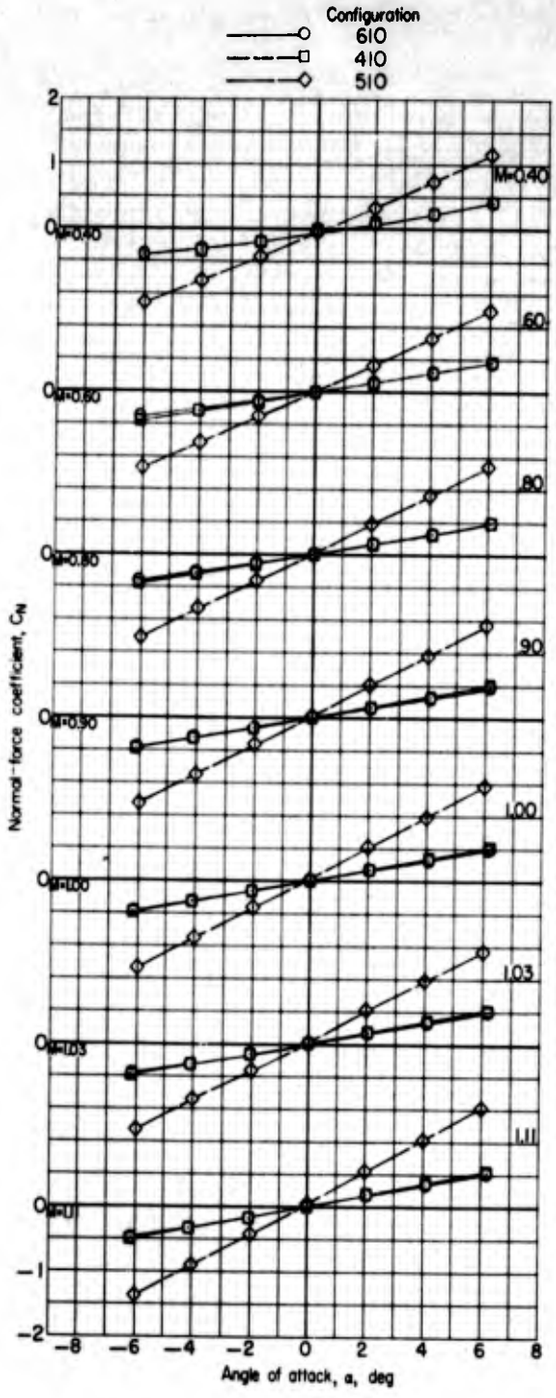

(a) C_N plotted against α.

Figure 13.- Effects of delta fins and protuberances on aerodynamic characteristics in pitch for configurations with flared-skirt afterbody. 1/10-scale three-stage Scout model.

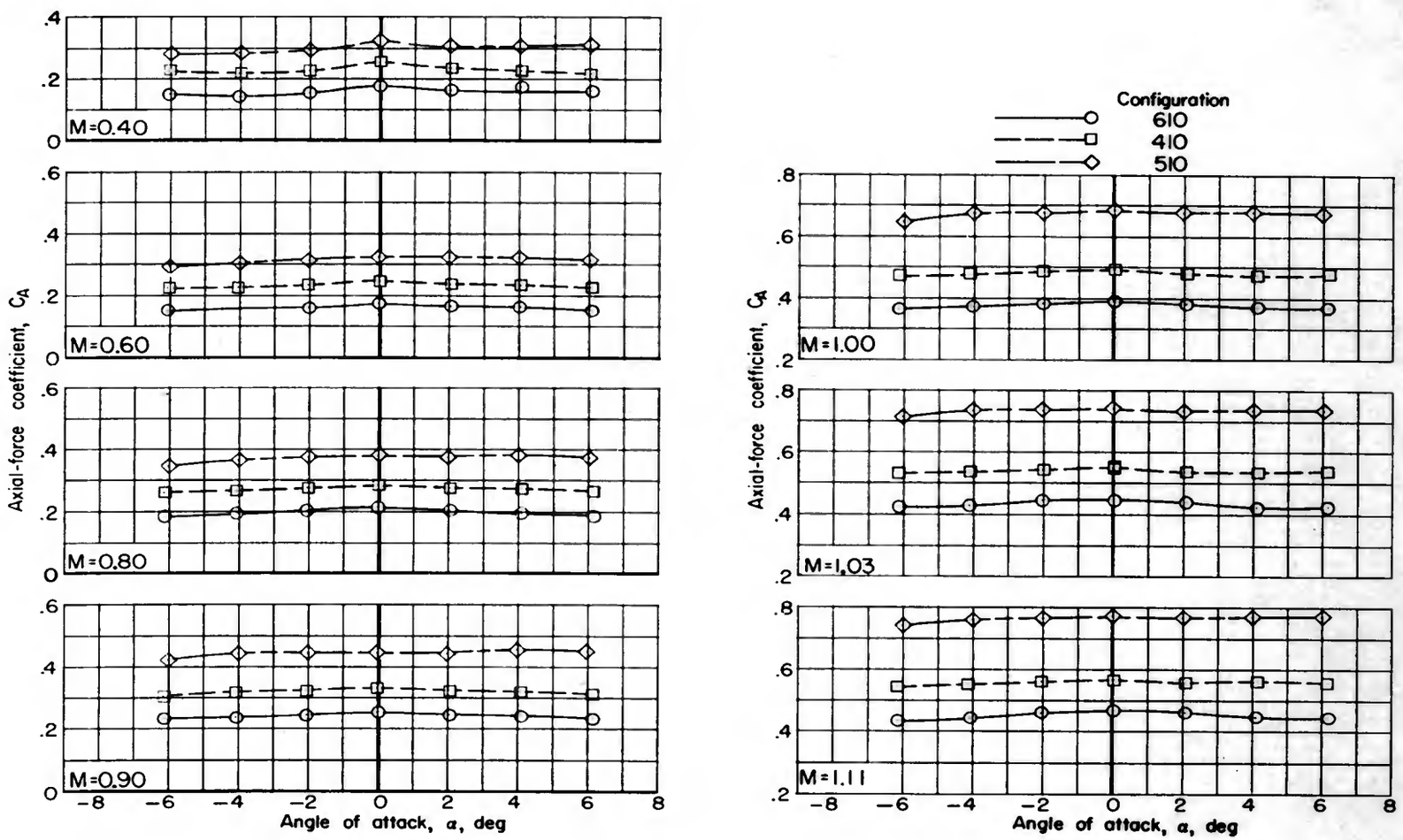

(b) C_A plotted against α.

Figure 13.- Continued.

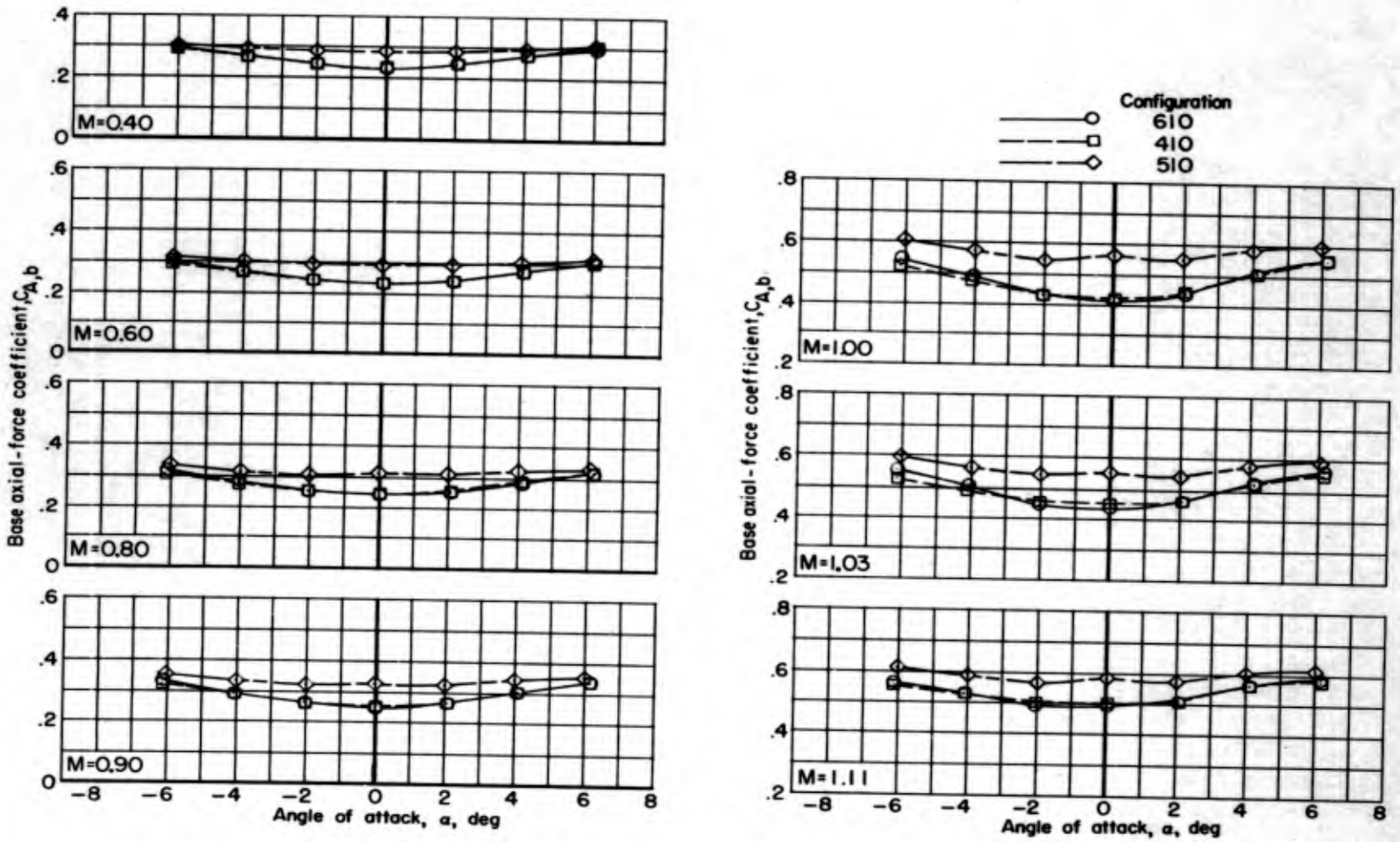

(c) $C_{A,b}$ plotted against α.

Figure 13.- Continued.

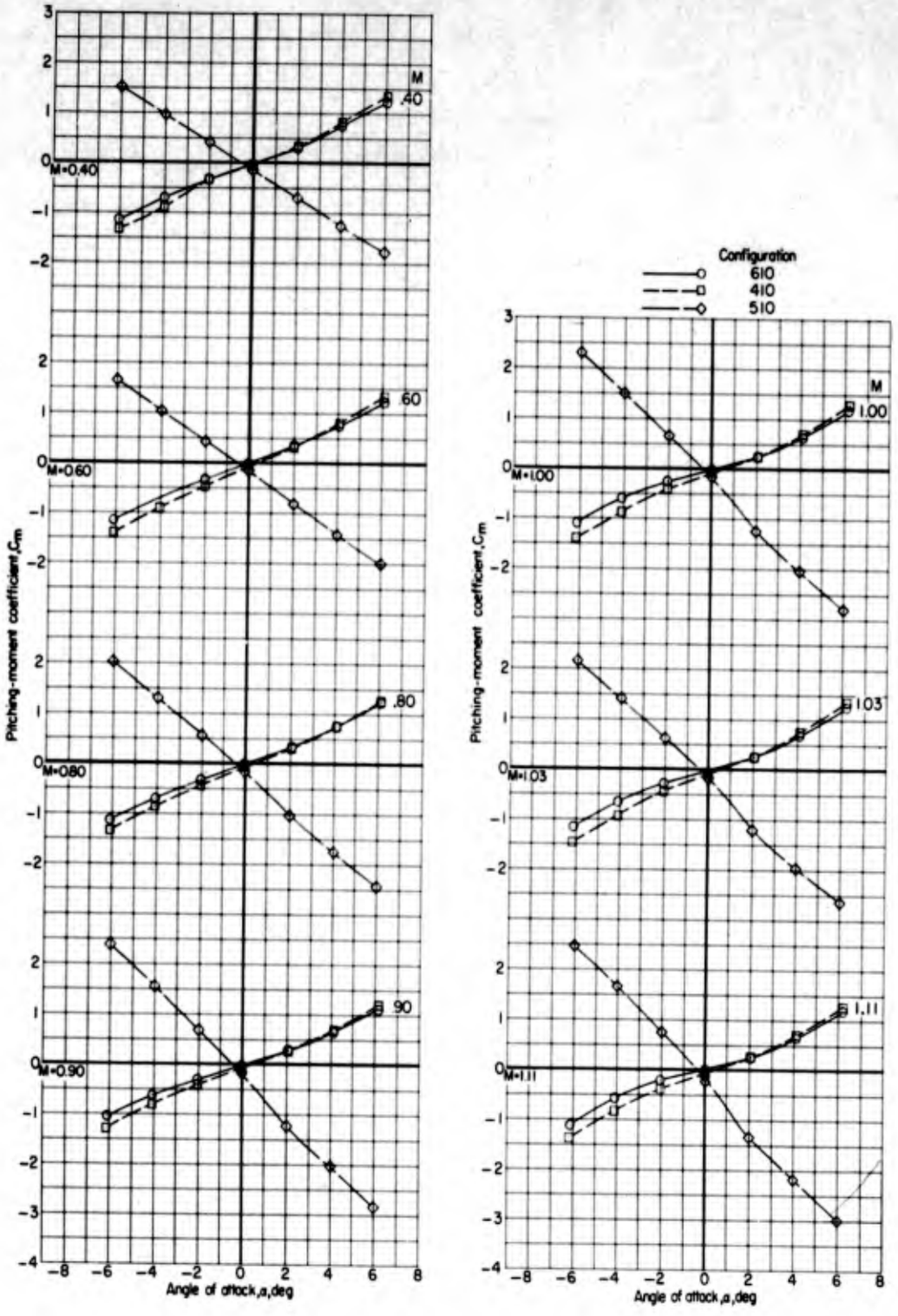

(d) C_m plotted against α.

Figure 13.- Continued.

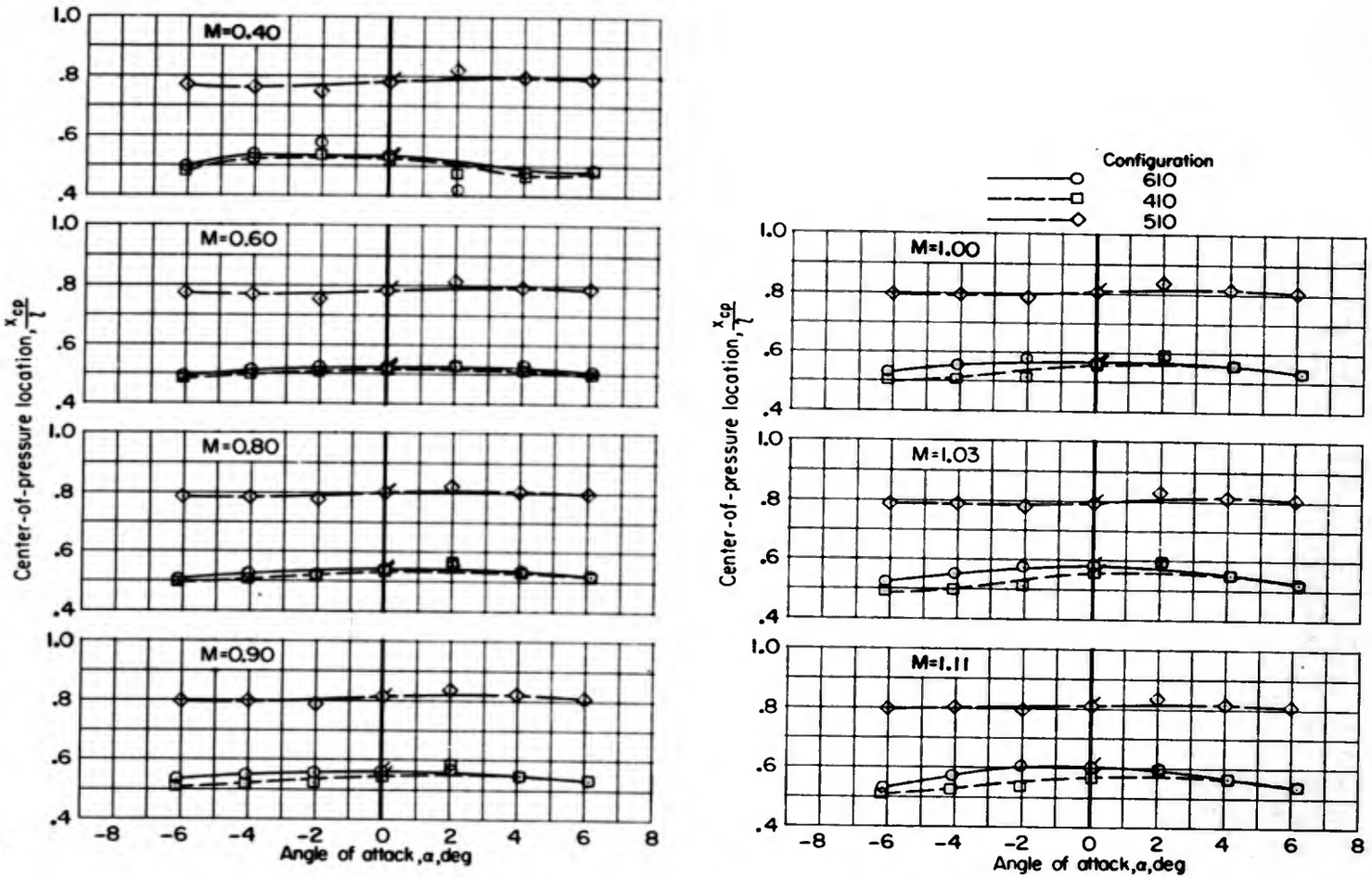

(e) $\frac{x_{cp}}{l}$ plotted against α.

Figure 13.- Concluded.

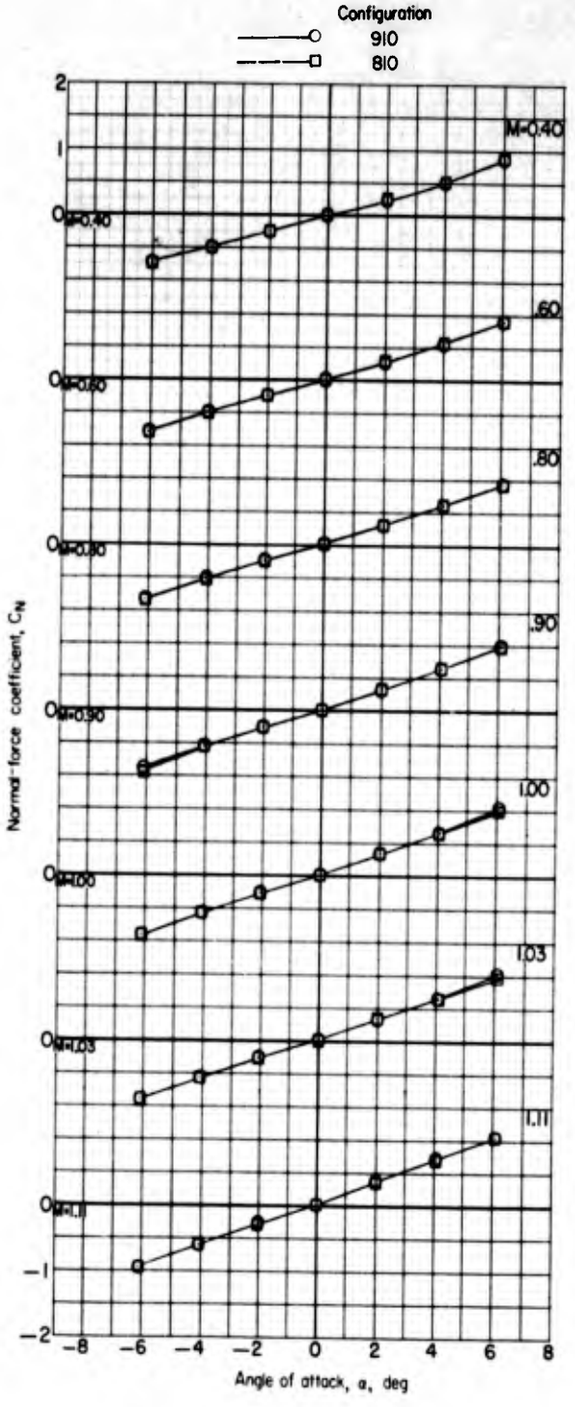

(a) C_N plotted against α.

Figure 14.- Effects of flared-skirt afterbody on aerodynamic characteristics in pitch for configurations with clipped delta fins. 1/10-scale three-stage Scout model.

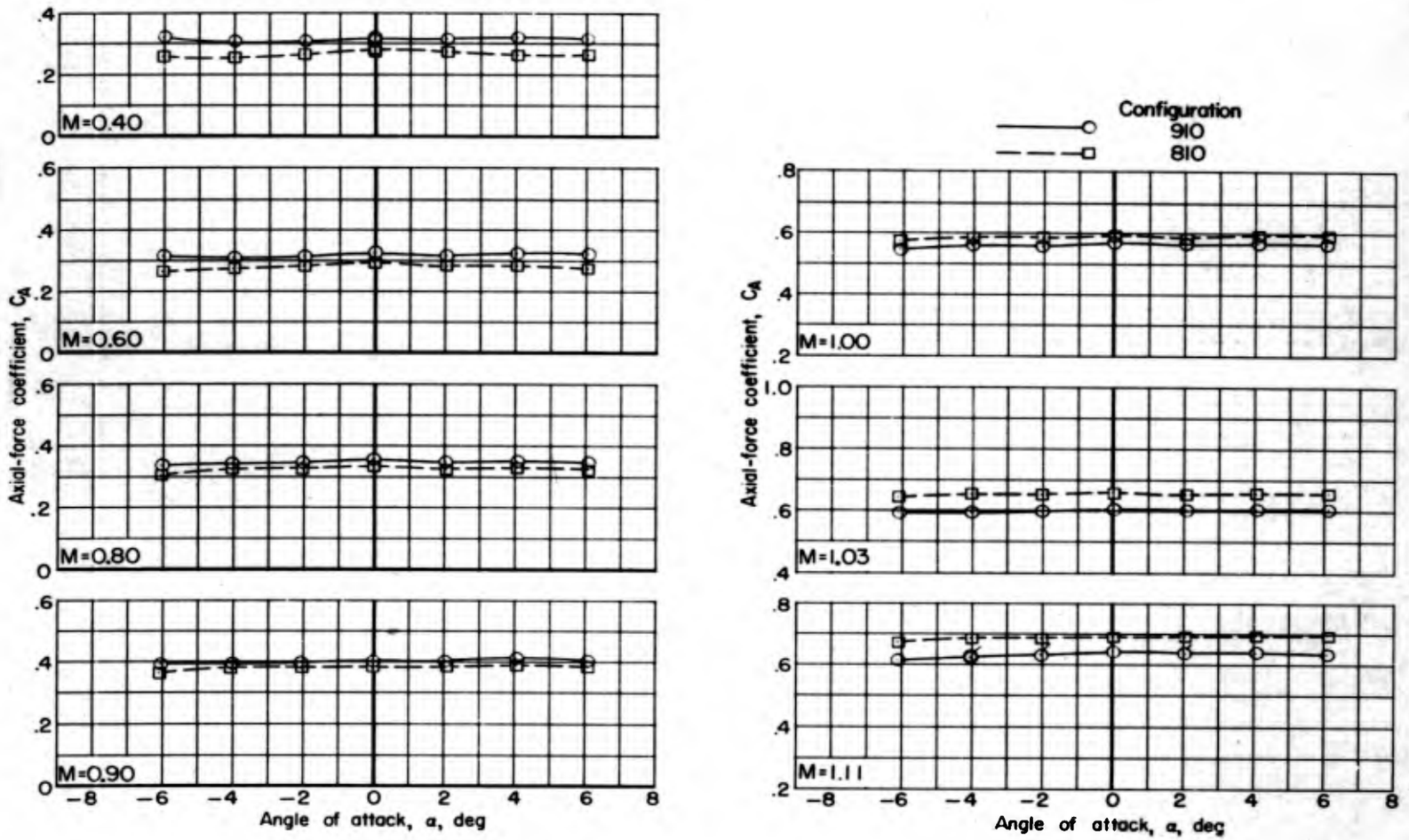

(b) C_A plotted against α.

Figure 14.- Continued.

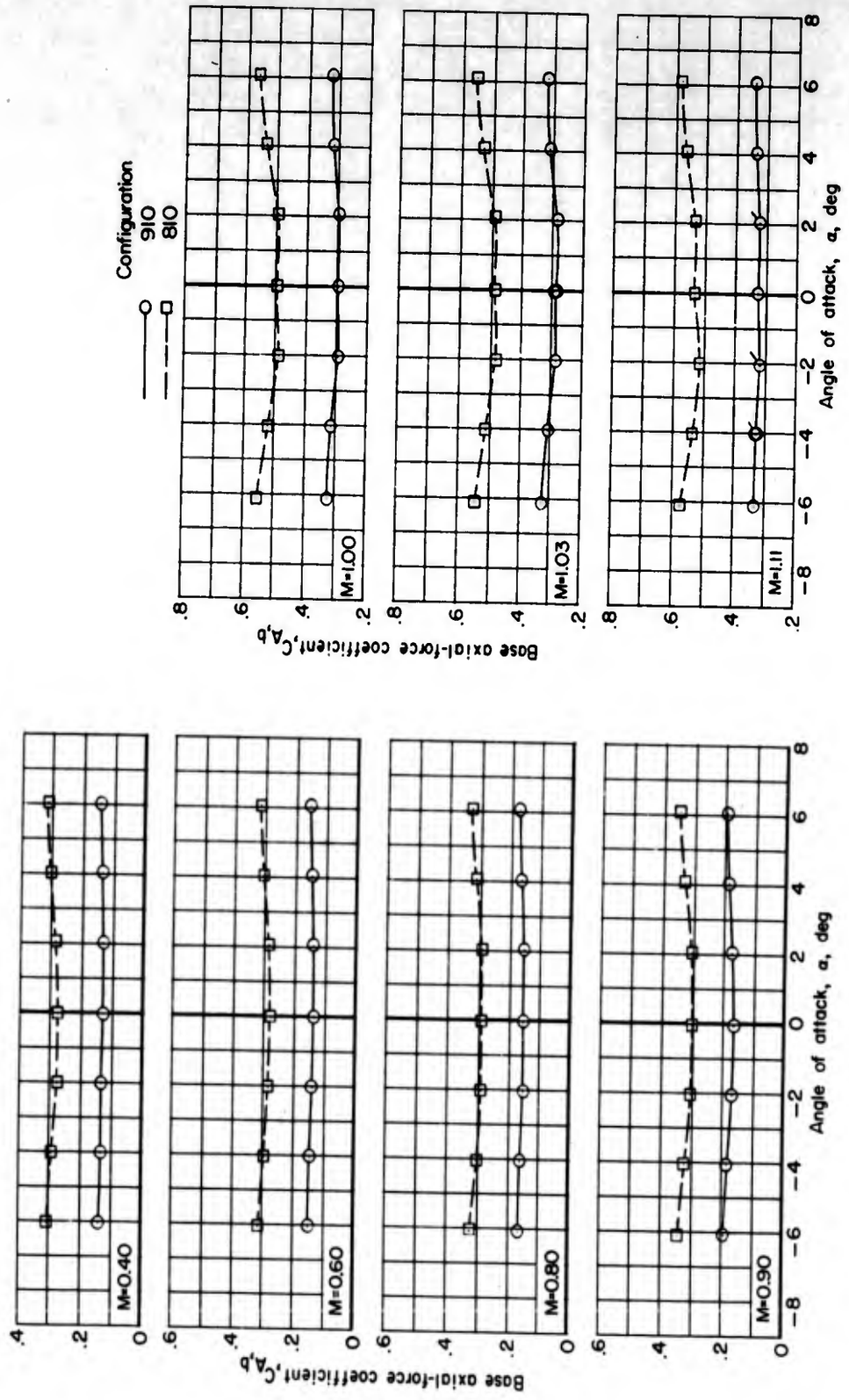

(c) $C_{A,b}$ plotted against α.

Figure 14.- Continued.

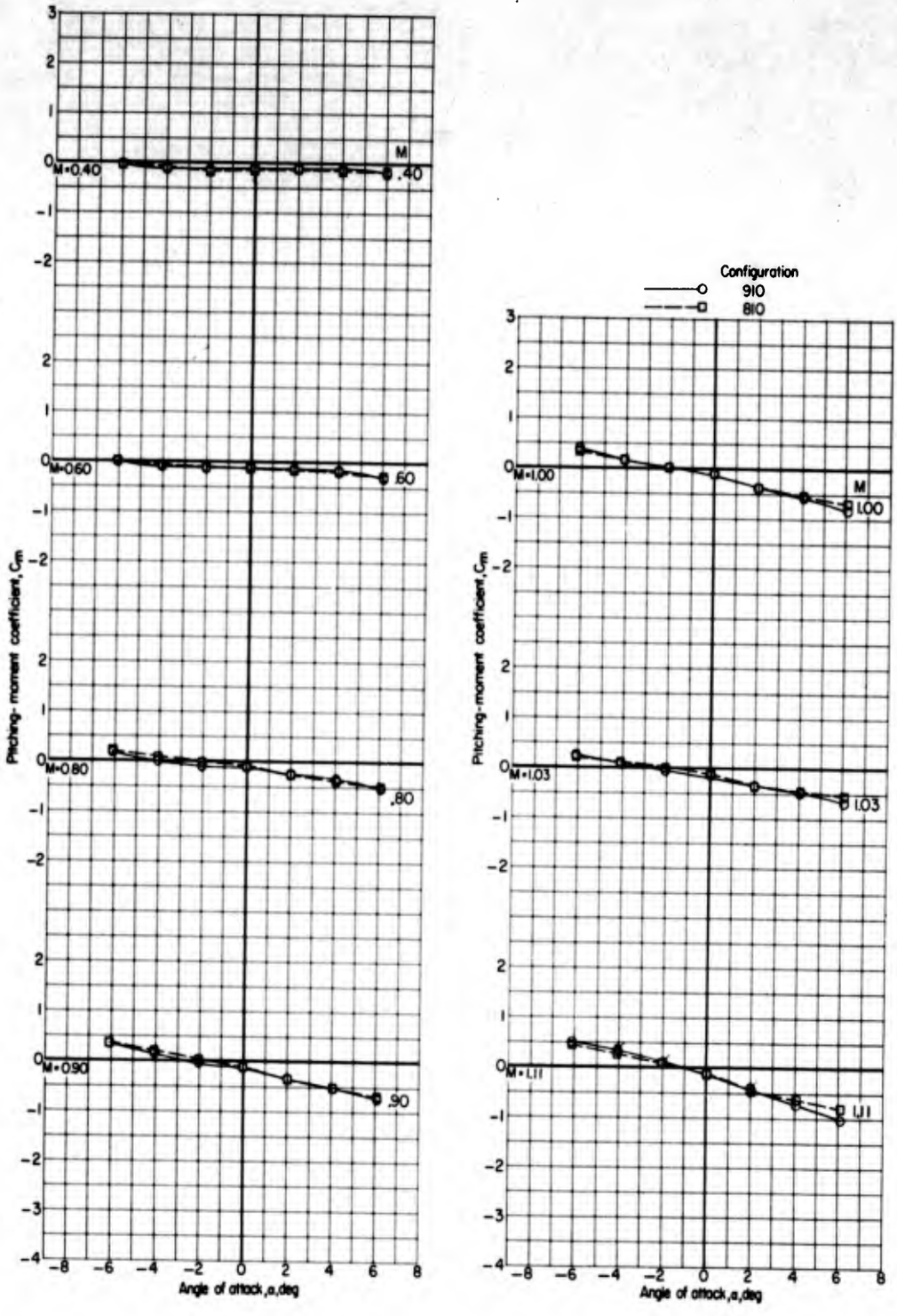

(d) C_m plotted against α.

Figure 14.- Continued.

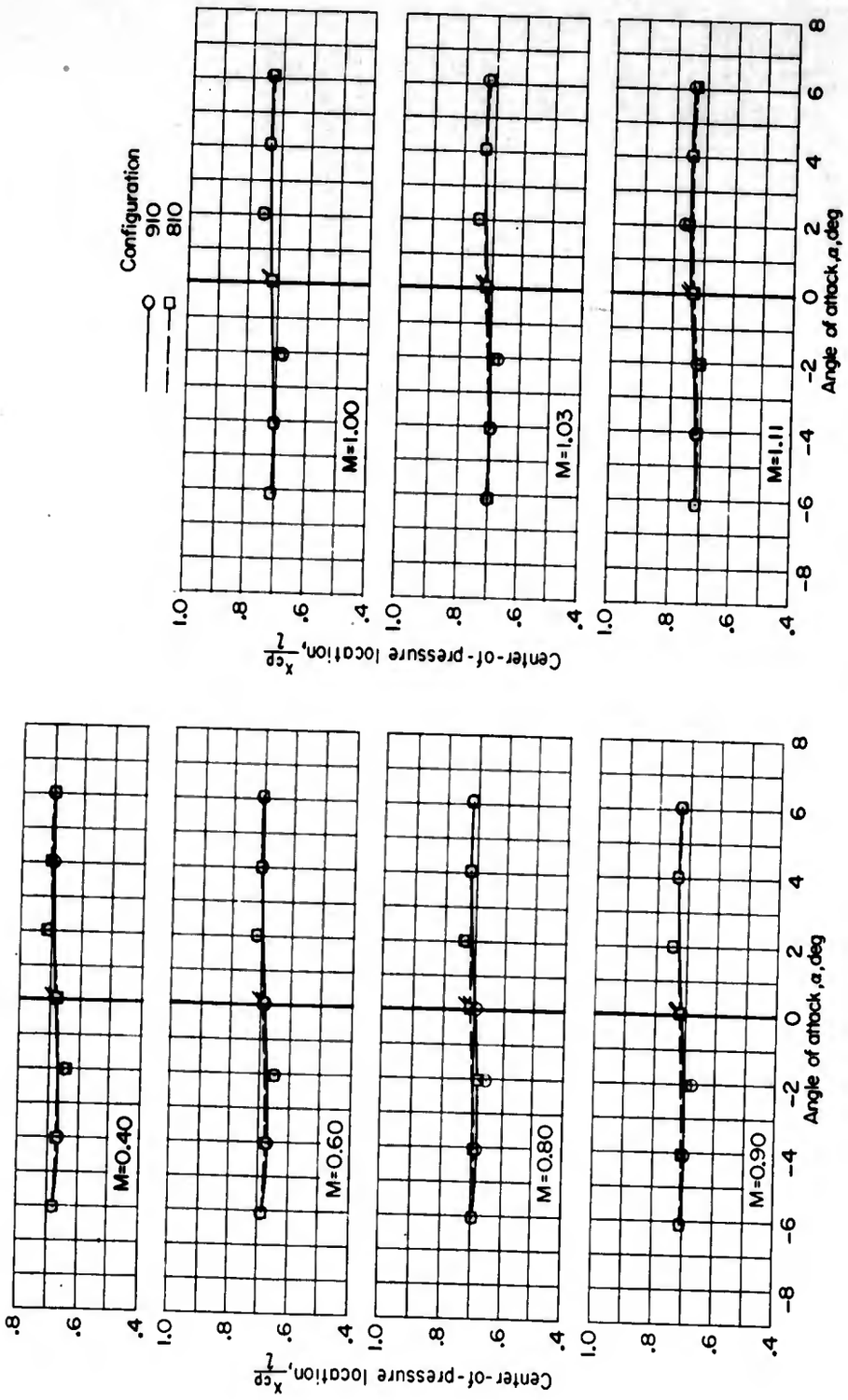

(e) $\frac{x_{cp}}{l}$ plotted against α.

Figure 14.- Concluded.

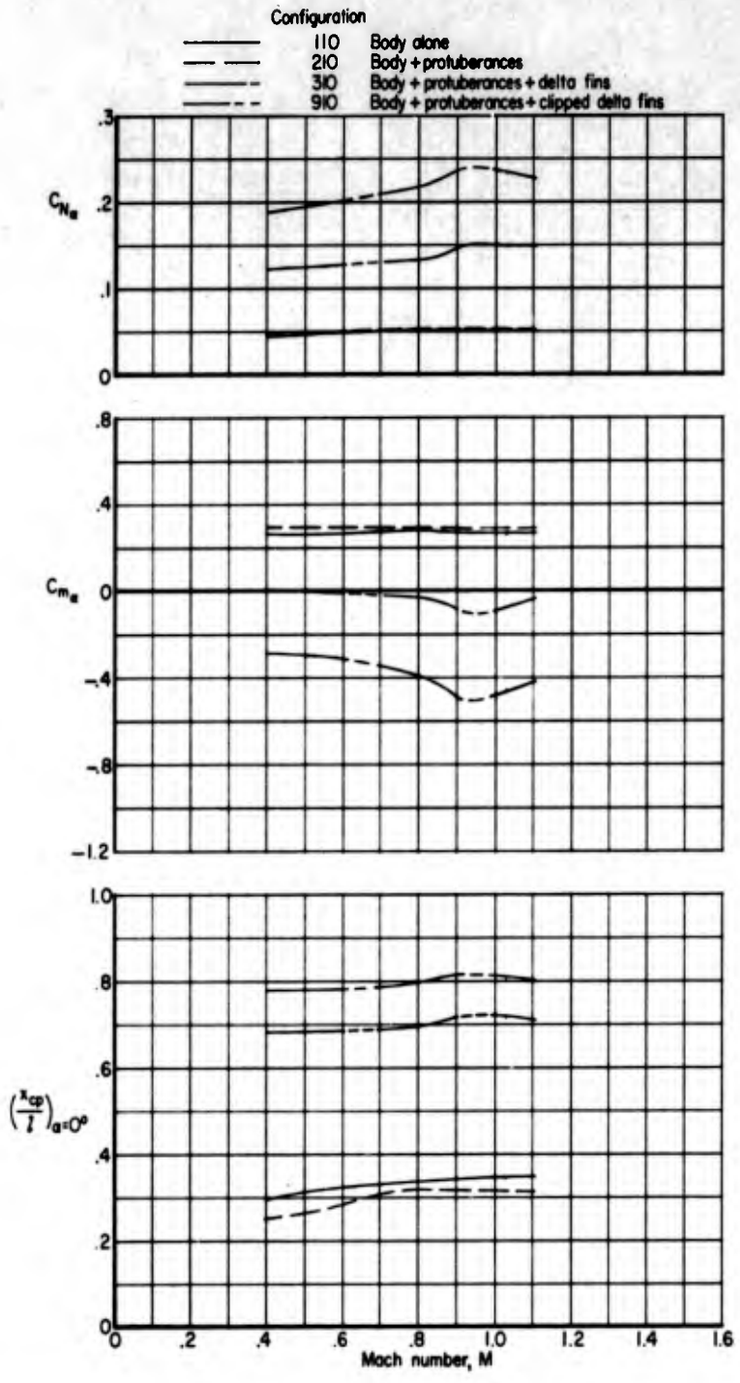

(a) C_{N_α}, C_{m_α}, and $\frac{x_{cp}}{l}$ plotted against Mach number. $\alpha = 0^\circ$.

Figure 15.- Summary of effects of fin planform and protuberances on aerodynamic characteristics in pitch for configurations with cylindrical afterbody. 1/10-scale three-stage Scout model.

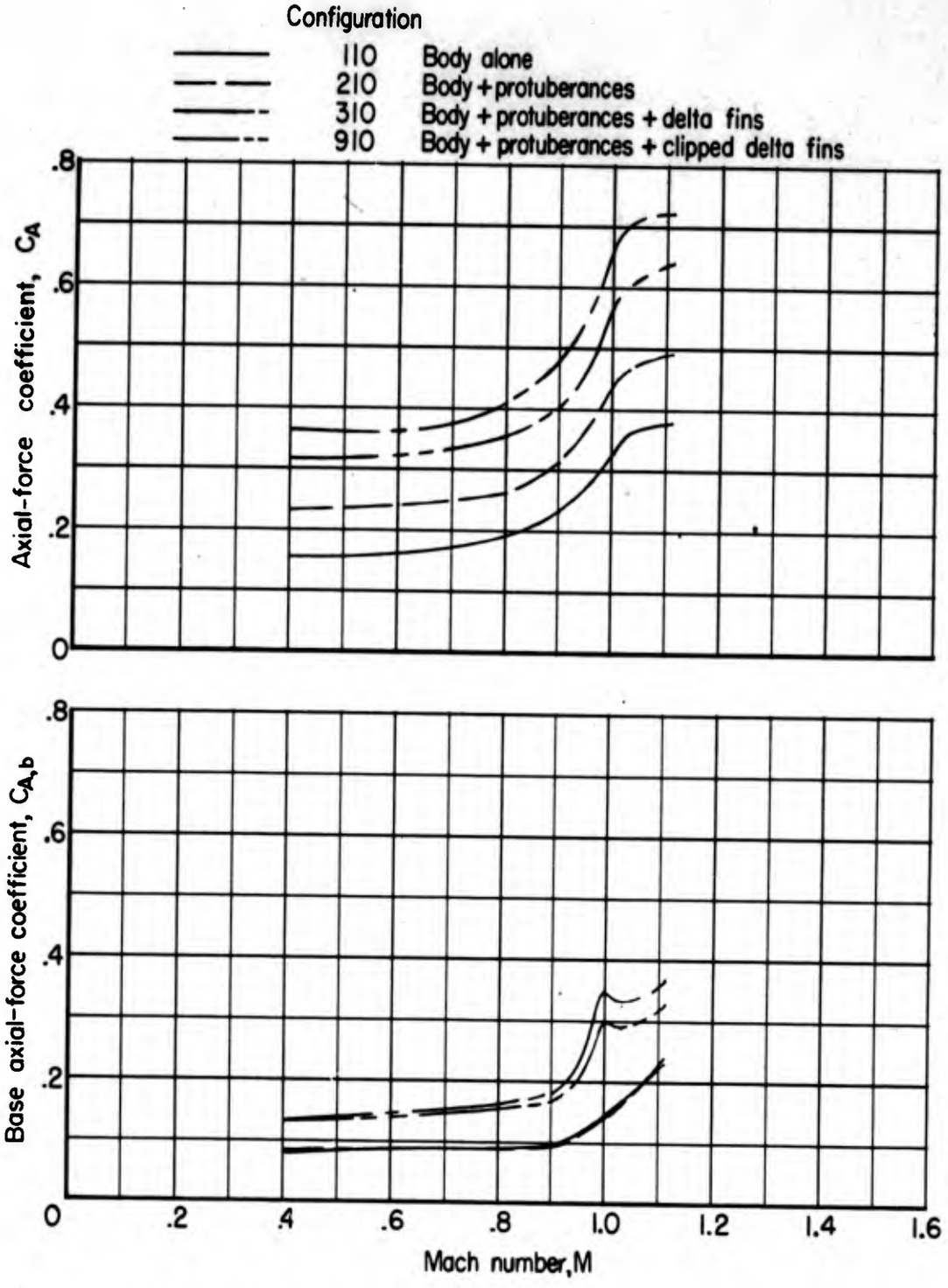

(b) C_A and $C_{A,b}$ plotted against Mach number. $\alpha = 0^\circ$.

Figure 15.- Concluded.

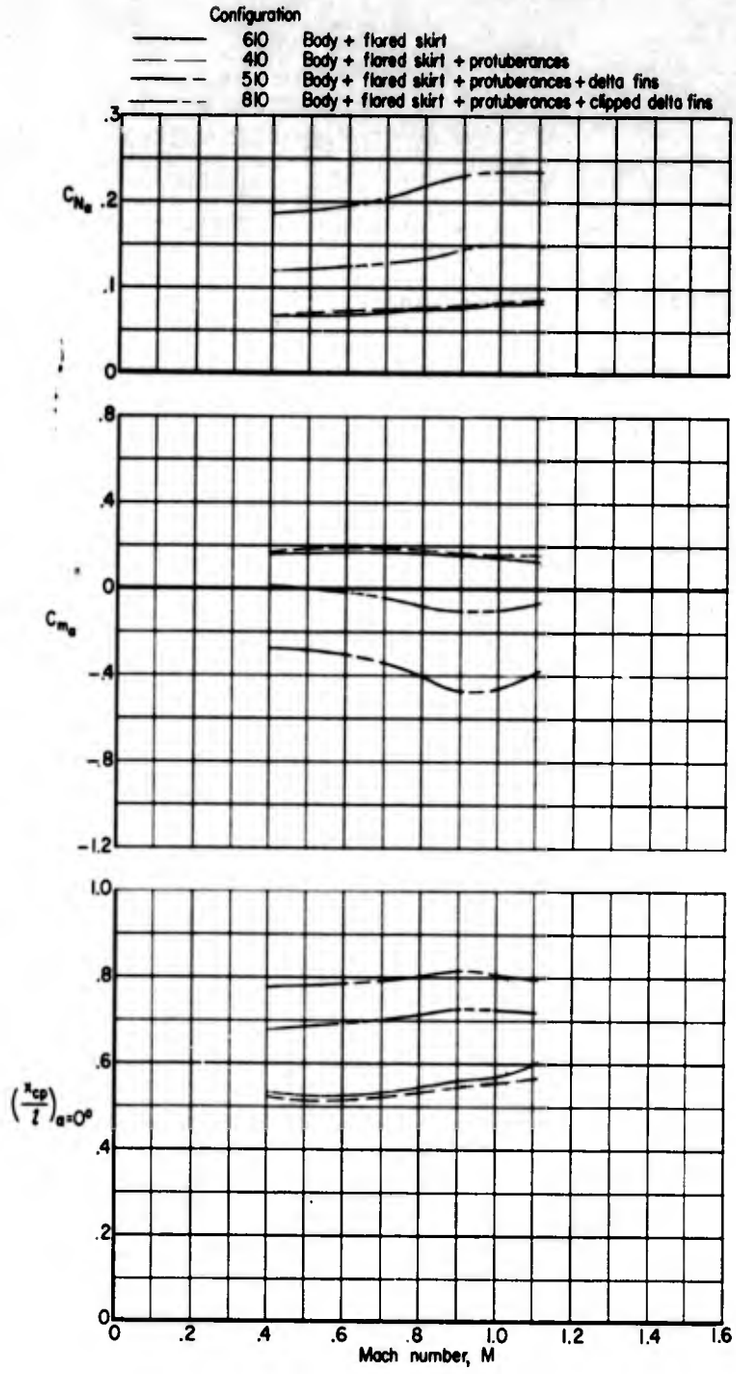

(a) C_{N_α}, C_{m_α}, and $\frac{x_{cp}}{l}$ plotted against Mach number. $\alpha = 0^\circ$.

Figure 16.- Summary of effects of fin planform and protuberances on aerodynamic characteristics in pitch for configurations with flared-skirt afterbody. 1/10-scale three-stage Scout model.

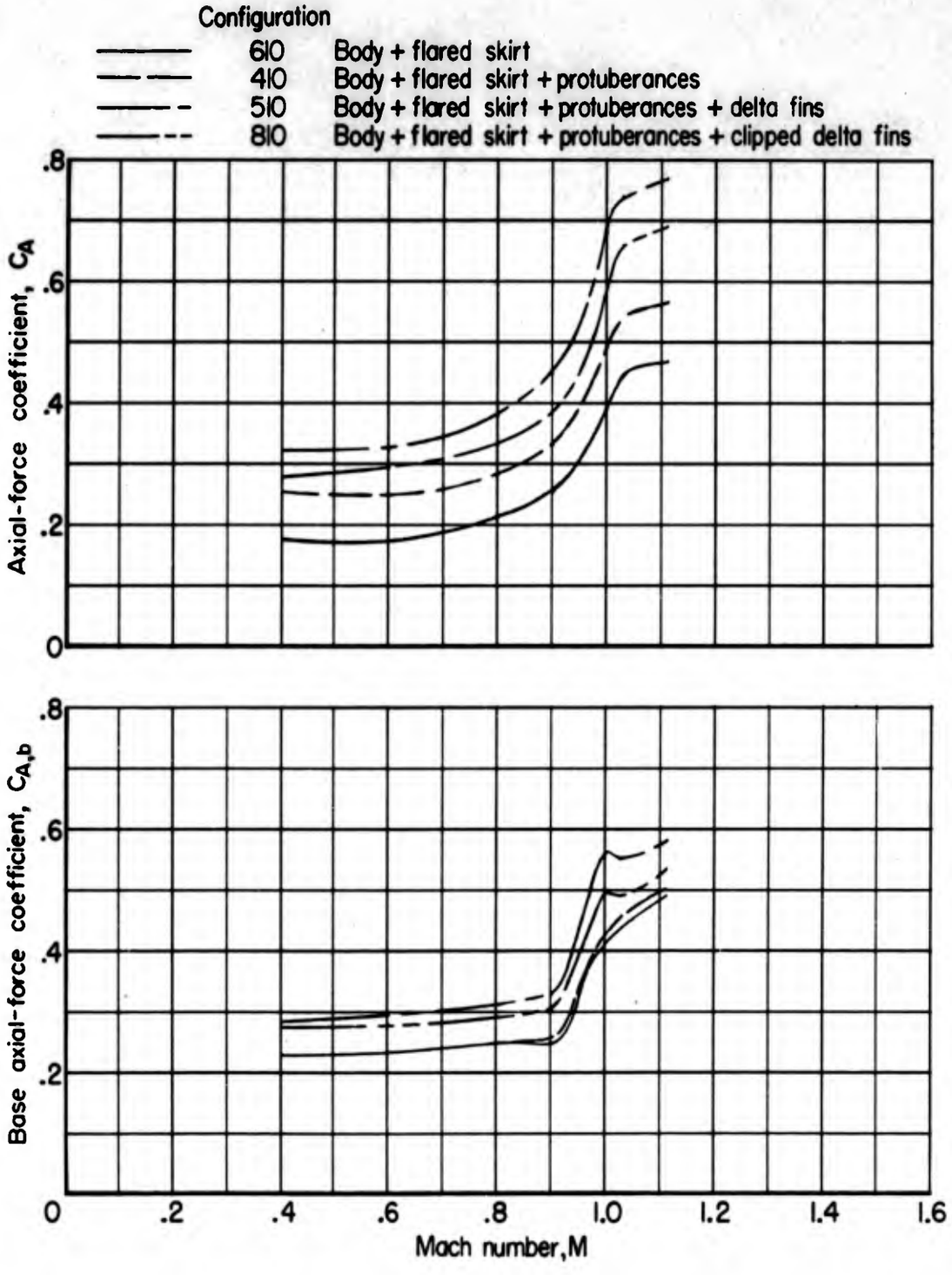

(b) C_A and $C_{A,b}$ plotted against Mach number. $\alpha = 0^\circ$.

Figure 16.- Concluded.

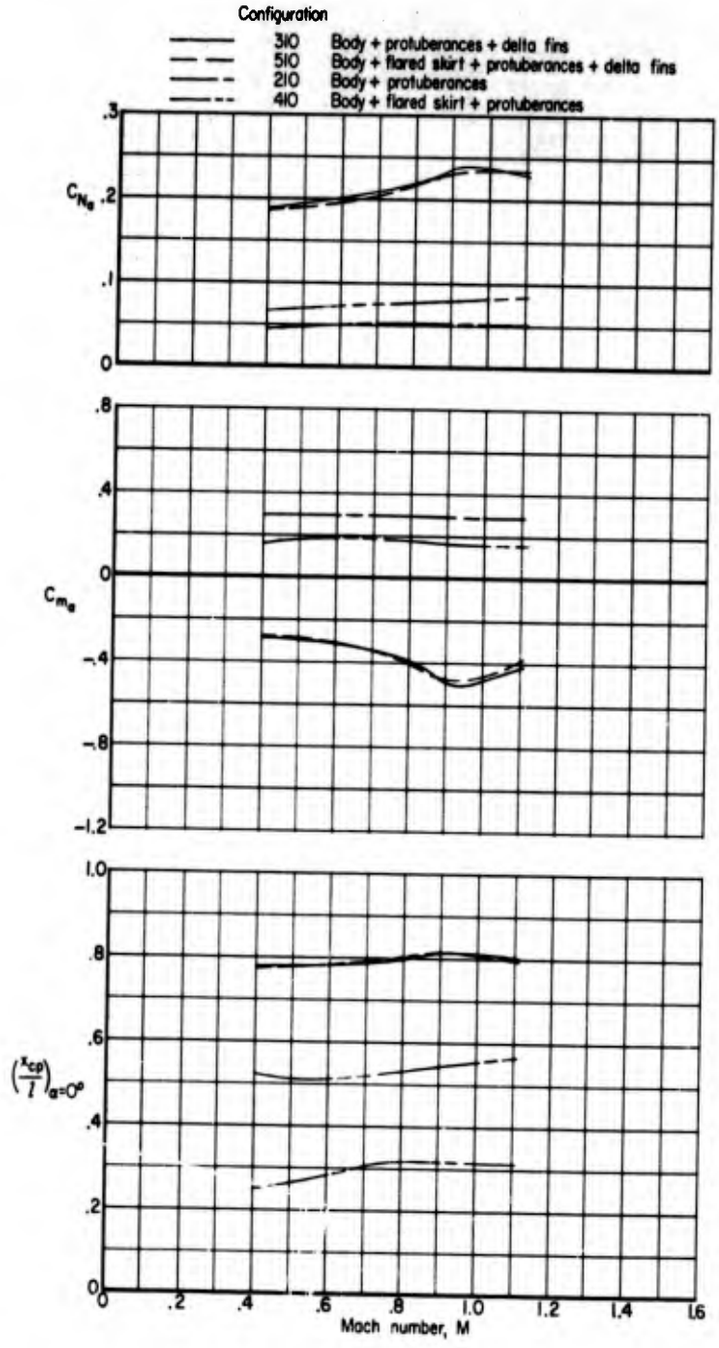

(a) C_{N_α}, C_{m_α}, and $\frac{x_{cp}}{l}$ plotted against Mach number. $\alpha = 0^\circ$.

Figure 17.- Summary of effects of flared-skirt afterbody on aerodynamic characteristics in pitch. Configurations of 1/10-scale three-stage Scout model.

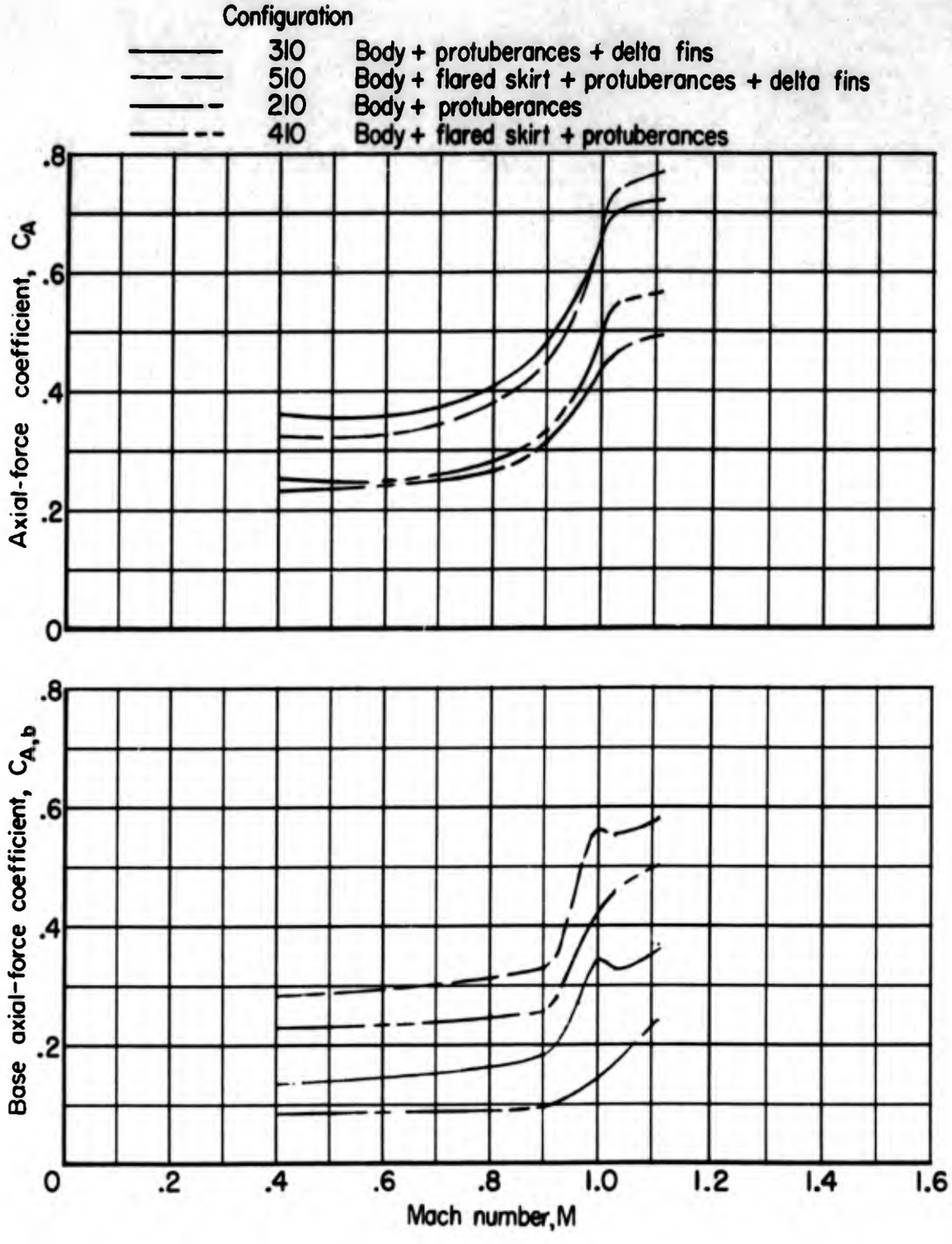

(b) C_A and $C_{A,b}$ plotted against Mach number. $\alpha = 0^\circ$.

Figure 17.- Concluded.

UNCLASSIFIED